Deep Mantle Seismic Modeling and Imaging

Thorne Lay[1] and Edward J. Garnero[2]

[1]Department of Earth and Planetary Sciences, University of California, Santa Cruz, Santa Cruz, California 95064; email: tlay@ucsc.edu

[2]School of Earth and Space Exploration, Arizona State University, Tempe, Arizona 85287-1404; email: garnero@asu.edu

Annu. Rev. Earth Planet. Sci. 2011. 39:91–123

First published online as a Review in Advance on January 27, 2011

The *Annual Review of Earth and Planetary Sciences* is online at earth.annualreviews.org

This article's doi:
10.1146/annurev-earth-040610-133354

0084-6597/11/0530-0091$20.00

Keywords

lower-mantle structure, D″, core-mantle boundary, ultralow-velocity zones, thermochemical anomalies, superplumes

Abstract

Detailed seismic modeling and imaging of Earth's deep interior is providing key information about lower-mantle structures and processes, including heat flow across the core-mantle boundary, the configuration of mantle upwellings and downwellings, phase equilibria and transport properties of deep mantle materials, and mechanisms of core-mantle coupling. Multichannel seismic wave analysis methods that provide the highest-resolution deep mantle structural information include network waveform modeling and stacking, array processing, and 3D migrations of P- and S-wave seismograms. These methods detect and identify weak signals from structures that cannot be resolved by global seismic tomography. Some methods are adapted from oil exploration seismology, but all are constrained by the source and receiver distributions, long travel paths, and strong attenuation experienced by seismic waves that penetrate to the deep mantle. Large- and small-scale structures, with velocity variations ranging from a fraction of a percent to tens of percent, have been detected and are guiding geophysicists to new perspectives of thermochemical mantle convection and evolution.

INTRODUCTION

Seismic waves generated by earthquakes and controlled sources provide the highest-resolution probes of Earth's interior structure below the ∼10-km maximum depth achieved by drilling. Elastic P and S waves spread outward in all directions from surface or underground sources of energy release, with velocities controlled by the incompressibility, rigidity, and density of minerals and fluids in the interior. These P and S waves reflect and refract from abrupt changes in material properties, eventually arriving at Earth's surface, where they can be recorded by seismometers (ground motion–recording instruments). Seismic wave travel time accumulates along the entire path traversed from source to receiver, providing integral constraints on seismic velocities along the path, whereas the existence and amplitudes of reflected phases constrain contrasts in material properties localized at internal boundaries between rocks of different properties or between rocks and fluids. Seismological characterization of the deep Earth involves a combined analysis of seismic wave travel times and amplitudes for direct and scattered P- and S-wave arrivals.

In general, seismic wave–travel time analyses of Earth's lowermost mantle resolve smooth, large-scale structures, whereas scattered-phase analyses resolve rough, small-scale structures and boundaries. The accuracy and detail to which the interior can be characterized depends strongly on the bandwidth of the recorded seismograms, the station spacing relative to the direction of wave propagation, the frequency of the waves, and the ray-path coverage of the medium provided by the spatial distribution of sources and seismometers. In the case of detailed seismic imaging of shallow crustal environments, land and/or oceanic deployments of thousands of seismometers and hundreds of controlled sources in two-dimensional (2D) distributions are used. Procedures for resolving both smooth and rough structures at shallow depths have been extensively developed for these dense data sets and provide the remarkable 2D and 3D crustal structural images used in oil and resource exploration, with resolution that approaches the scale of geological formations. As the targeted imaging depth increases, structural resolution diminishes as a result of (*a*) loss of signal bandwidth due to anelastic attenuation of the seismic waves and (*b*) reduced ray-path spatial sampling of the medium of interest due to significant limitations of the configurations of sources (typically earthquakes) and stations (typically land-based). Seismic waves from shallow sources that penetrate ∼2,890 km deep to Earth's core-mantle boundary (CMB) travel immense path lengths thousands of kilometers long through attenuating and heterogeneous rock layers before being recorded at the surface, and they require a more expanded recording aperture compared with that used in crustal investigations to accommodate the higher-wave velocities and larger structural targets present at greater depths. Although deep mantle imaging cannot achieve the quality and resolution typical in oil exploration work, recent expansion of many seismic networks and ease of data availability have resulted in increased use of more sophisticated data-processing methodologies. In this review, we consider advances in our understanding of deep mantle structure over the past decade (see Garnero 2000 for a review of earlier work), emphasizing developments from the continuum of high-resolution methods ranging from waveform modeling to stacking and migration, all of which exploit systematic behavior of wave interactions with deep velocity heterogeneity.

There are many motivations for determining detailed seismic velocity structures of the deep mantle. Although smooth, large-scale (>500–1,000 km) global mantle structures continue to be refined through the use of seismic wave–travel time tomography (e.g., Ritsema & van Heijst 2000, Gu et al. 2001, Grand 2002, Antolik et al. 2003, Zhao 2004, Panning & Romanowicz 2006, Takeuchi 2007, Kustowski et al. 2008, Li et al. 2008) and some consistency is emerging, particularly among S-wave velocity models, there are intrinsic ambiguities in attributing the smooth components of seismic velocity variations to effects of temperature, composition, or anisotropic fabric.

Simultaneous inversion for P- and S-wave velocities—and if possible, density—can overcome some of the ambiguities, but essential information about the geological processes (melting, shearing, folding, stratification, phase transitions, transport properties) is more directly manifested in the rough, fine-scale structural information revealed by seismic wave reflections and scattering, similar to the information manifested in a heterogeneous crustal environment. Fundamental attributes of the boundary layer at the base of the mantle such as the distribution of chemical heterogeneities, flow structures, and zones of partial melting can be only marginally sensed, if at all, by methods that map large-scale mantle structure. Detailed information can be extracted through the direct modeling of visible secondary arrivals or waveform distortions of principle seismic phases, as discussed in the next section. However, the seismic wave manifestations of complexities in the deep mantle often involve subtle features that can be difficult to detect and quantify. This motivates the use of robust procedures to extract weak arrivals amid a background of ambient noise, similar to procedures used in shallow seismic exploration applications (e.g., Rost & Thomas 2002).

DEEP MANTLE SEISMIC MODELING AND IMAGING CHALLENGES

We focus on determinations of structures in the deep mantle, by which we mean the ~1,000 km of the lower mantle directly overlying the CMB. The lowermost ~200–300 km of the lower mantle is formally designated the D″ region (Bullen 1949) because of its long-recognized departures from the seismic homogeneity expected for uniform composition material under self-compression. The D″ region has generally been associated with a thermal boundary layer at the base of the mantle produced by heat fluxing out of the much hotter core, and possibly with a concentration of dense materials from the mantle (or light materials from the core) that have segregated throughout Earth history (Lay & Garnero 2004, Labrosse et al. 2007, Garnero & McNamara 2008, Trønnes 2009). Approximately a decade ago, studies established that some deep mantle structures may extend upward ~800–1,000 km from the CMB with a distinctly red (long wavelength–dominated) heterogeneity spectrum (e.g., Ritsema et al. 1998, Ishii & Tromp 1999, Kellogg et al. 1999, van der Hilst & Kárason 1999, Garnero 2000); we thus define this thicker region to be the deep mantle of interest here.

Although basic principles of determining seismic velocity structure that hold for shallow crustal structure also apply in deep mantle studies, many distinct challenges confront efforts to resolve detailed deep structure. Foremost is the need to use earthquakes as sources of seismic waves that can penetrate deeply into the planet; this requirement greatly limits the spatial configuration and increases the variability of the sources relative to shallow controlled-source applications. Corresponding constraints on receiver locations tend to result in irregular global-network observatory configurations that are largely confined to continents that have large interstation spatial separations. In many investigations, regional networks or dense arrays of stations with smaller separations have been used to study deep structure, but typically these have a small spatial aperture or relatively short site occupancy (18–24 months) and commonly provide limited azimuthal sampling of localized deep mantle regions of interest. As noted above, the signals sampling the deep mantle must propagate thousands of kilometers downward and upward through shallower rock layers. These signals lose high-frequency energy owing to intrinsic attenuation, which generally limits the maximum signal frequencies to less than ~0.3–1 Hz. In the deep mantle, this implies P- and S-wave signal wavelengths no shorter than ~7–40 km, values that intrinsically delimit resolution of any fine structures that may be present. One of the key strategies of exploration seismology is to strive toward sampling each position in the imaged medium with waves of different incidence angles and azimuths; this is possible to a limited degree in only a few regions of the deep mantle owing to the constraints on source and receiver distributions. Multiple ray-path sampling of the same region also requires use of many earthquakes with variable source signals that must be equalized in the modeling. The great depth of lower-mantle structures, the tendency of most seismic imaging methods to preferentially sense quasi-horizontal boundaries, and the small contrasts in material properties involved (typically only a few percent except just above the CMB) motivate the combination of information from precritical angles of incidence (involving weak reflections of seismic waves mainly sensitive to impedance contrasts) and postcritical angles of incidence (involving large but grazing triplications with phase-shifted reflections mainly sensitive to velocity contrasts). Seismic wave reflection and conversion coefficients from seismic velocity gradients and discontinuities that depend on ray geometry, material density, and seismic velocities produce complex wave behavior, which complicates imaging applications. Fully elastic wave calculations are required in most cases, whereas shallow applications can often utilize acoustic wave approximations.

To address some of these imaging difficulties, lower-mantle studies have employed a diversity of seismic phases (**Figure 1**) that sample deep structure as fully as possible, notably including conversions of P and S waves that are usually ignored or suppressed in shallow exploration applications. Only a handful of portable instrument deployments have been designed primarily for deep mantle studies. However, the open availability of continuous broadband seismic data from international seismic observatories and portable instrument deployments provided by the Incorporated Research Institutions for Seismology (IRIS) and International Federation of Digital Seismograph Networks (FDSN) data centers, as well as seismic data from regional earthquake monitoring networks, enables substantial data sets to be brought to bear on deep mantle investigation, irrespective of what originally motivated the instrument deployments. Large seismogram data sets (as in **Figure 2**) have been essential for advancing the determinations of deep mantle structure considered here. We begin by briefly considering recent travel time investigations because they commonly frame the detailed modeling and imaging applications for the deep mantle.

MULTIPLE-ARRIVAL TRAVEL TIME APPROACHES

Almost all seismic wave investigations of deep mantle structure utilize a reference 1D model of seismic wave velocities and density as a function of depth, such as the Preliminary Reference Earth Model (PREM) (Dziewonski & Anderson 1981). 1D reference models have smooth velocity increases with depth across the lower mantle and, commonly, reduced rates of increase in the lower few hundred kilometers of the mantle (or even slightly negative velocity gradients). These are followed by a large, discontinuous drop in P-wave velocity, a vanishing of S-wave velocity, and a large increase in density across the CMB near 2,900-km depth. Even a simple 1D model predicts substantial complexity of the wavefield owing to top- and bottom-side reflections and conversions of wave energy at the sharp CMB (**Figure 1**), along with diffractions of grazing wave energy (e.g., Garnero 2000). These complexities are predictable through the use of 1D model ray tracing and synthetic waveform computation methods that were developed in the 1970s. The methods provide reference signal predictions relative to which actual data complexities (like those in **Figure 2**) can be juxtaposed, and localized 1D, 2D, or 3D models can be developed.

Seismic tomography usually exploits the travel time fluctuations of the major phases predicted for a 1D model to invert for perturbations relative to the reference structure; it does so through a set of basis functions (e.g., polynomials, splines, volume elements) to represent the 3D velocity perturbations in the medium. The deep mantle may be characterized as part of a global mantle inversion or a separate target of tomography desensitized to shallower structure by use of differential arrival times between direct phases (e.g., P, S, PKP, SKS) and CMB-reflected phases (e.g., PcP, ScS, PKKP, SKKS). Depending on the source-receiver paths involved, the travel time imaging may involve localized deep regions (e.g., Bréger et al. 2001, Saltzer et al. 2001, Wysession et al.

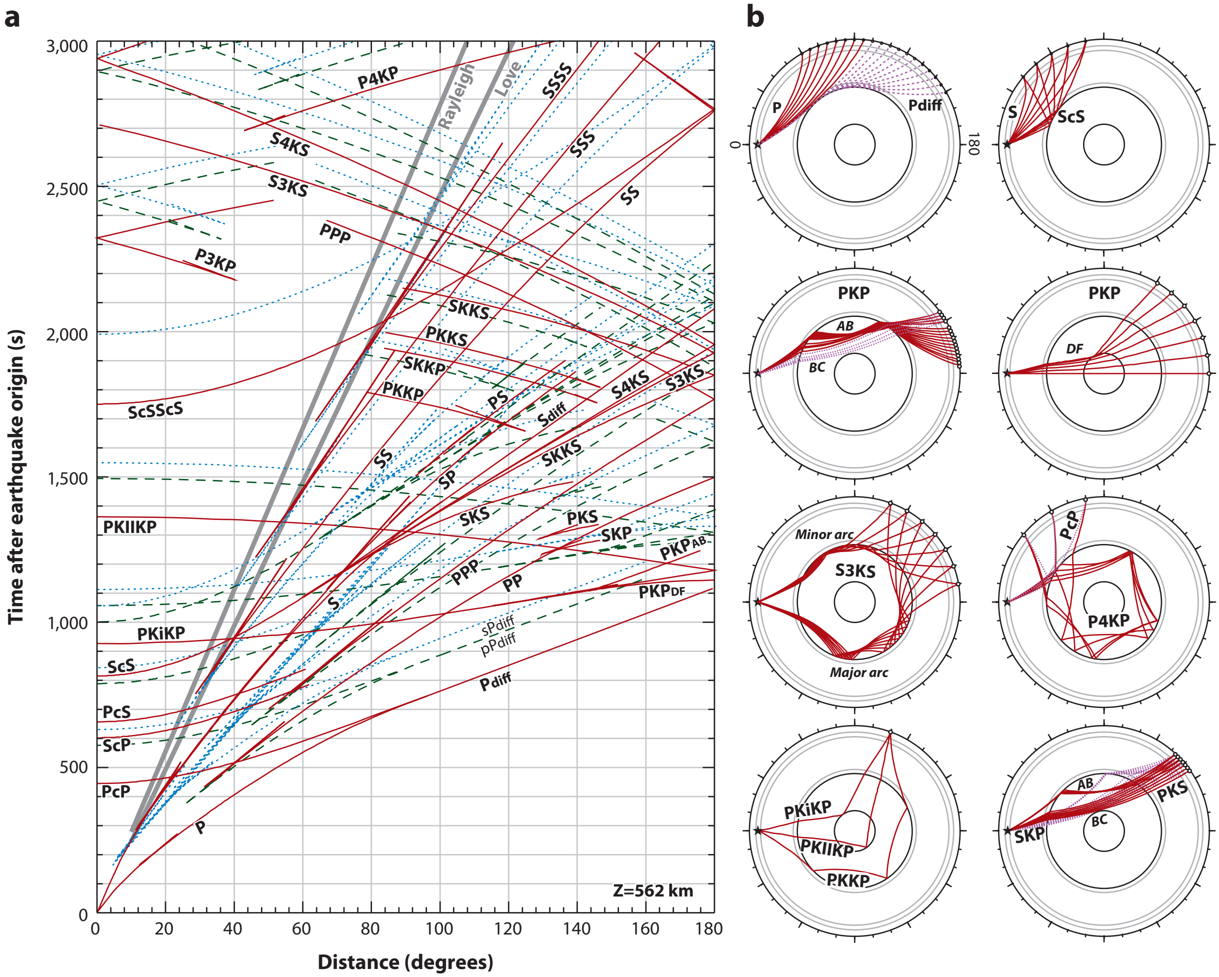

Figure 1

(*a*) Global travel time curves for the many of the seismic phases generated by a 562-km deep source in Preliminary Reference Earth Model (PREM), the 1D reference Earth model from Dziewonski & Anderson (1981). Dashed and dotted curves are upward-radiated P and S wave surface reflections (e.g., pPdiff and sPdiff). (*b*) Corresponding ray paths for specific phases commonly used in studies of the lowermost mantle and the core-mantle boundary. These arrivals are used in travel time tomography, waveform modeling, array processing, and migrations to determine deep mantle structure. The internal circles, from the outside in, represent the velocity discontinuities at 410 km, 660 km, and 2,700 km, the 2,891-km core-mantle boundary, and the 5,150-km deep inner core–outer core boundary.

2001, Simmons & Grand 2002, Tanaka 2002, Fisher et al. 2003, Garnero & Lay 2003, Hung et al. 2005, Wright & Kuo 2007) or global representations for deep mantle structure (e.g., Castle et al. 2000, Kuo et al. 2000). These focused deep mantle tomography studies reduce the horizontal resolution of structure from the >500–1,000-km scale in global tomography down to several hundred kilometer scale lengths. Most tomographic inversions are heavily damped, and the resulting structures only slightly perturb the ray paths of the major phases; synthetic waveform predictions from such long-wavelength models generally do not contain additional arrivals such as reflections and triplications that are observed in seismic data. 3D tomography models are increasingly used as

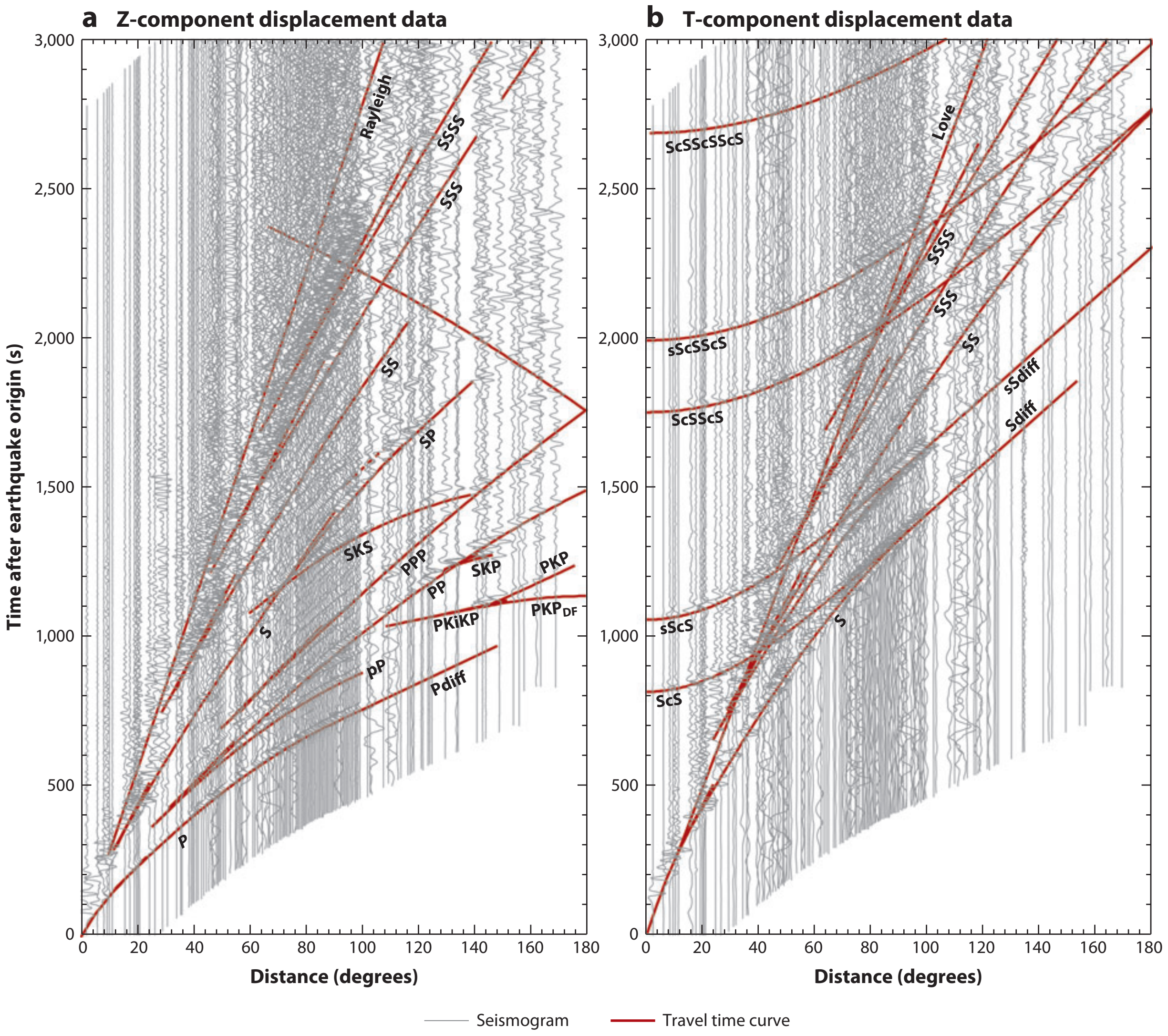

Figure 2

(*a*) Vertical- (Z-) and (*b*) tangential- (T-) component ground-displacement seismograms from a February 18, 2010, earthquake (42.6°N, 130.8°E, 01:13:00 UTC, m_b 6.7) 562 km deep beneath the Russia/China border region, low-pass filtered at a 20-s period and reduced in numbers to have one trace in each 0.5° distance interval. Selected travel time curves for Preliminary Reference Earth Model (PREM) (from **Figure 1**) are superimposed, with major phases labeled. Expansion of global networks of broadband seismometers in permanent observatories and in temporary deployments is providing huge data sets for imaging deep mantle structure.

a reference structure for deep mantle studies, but arbitrarily bolstering the amplitudes of the tomographic velocity anomalies to account for differential times of specific data sets often proves necessary.

If tomography is to include more complex layering than that featured in the standard reference models, the structure must be specified a priori, given that introduction of a velocity discontinuity has a nonlinear effect on the wavefield as it generates reflected or triplicated phases with distinct ray paths and travel time anomalies. Guided by long-standing evidence for an S-wave velocity

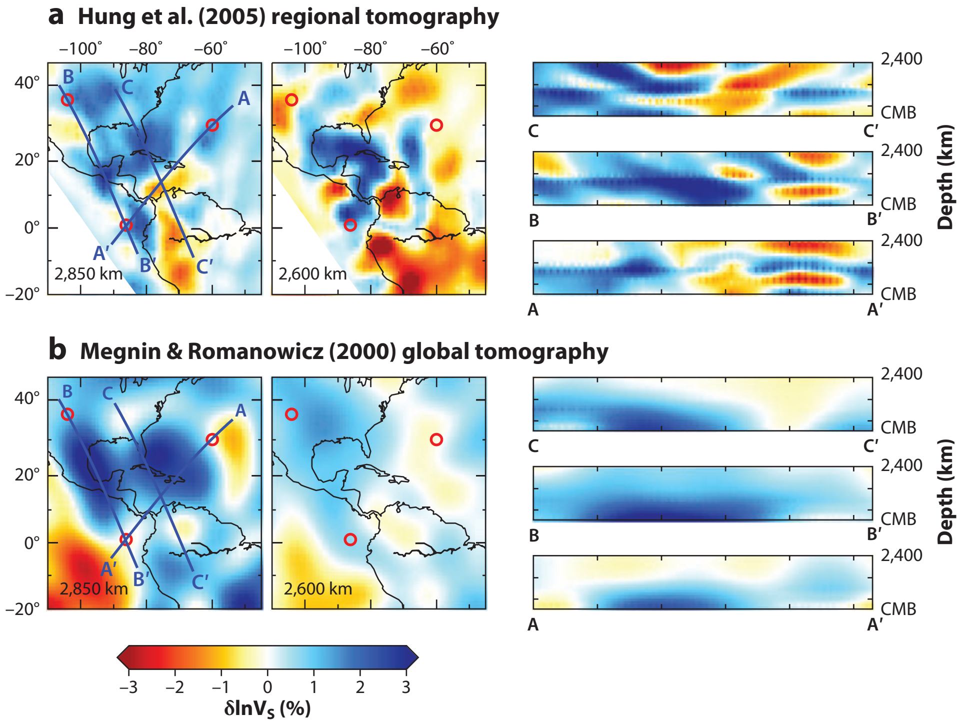

Figure 3

S-wave velocity variation relative to the Preliminary Reference Earth Model from (*a*) the regional finite-frequency tomography model of Hung et al. (2005) and (*b*) the global mantle tomography model of Megnin & Romanowicz (2000). The regional tomography model study incorporated a reference model containing a D″ discontinuity that produces triplication arrivals for which differential travel times relative to the core reflection were measured and included. This enhances the vertical resolution of structure in the region along with the use of a higher-resolution imaging grid. The leftmost two panels of each row illustrate the shear velocity fluctuations at the two depths indicated on the maps and on three great-circle cross sections, A–A′, B–B′, and C–C′. The red circles indicate the locations of surface hotspots in the Galapagos, Raton, and Bermuda. CMB, core-mantle boundary.

increase at the top of D″ in some regions (Lay & Helmberger 1983a), Hung et al. (2005) used a 1D reference structure with a 2.9% S-wave velocity discontinuity 250 km above the CMB in a regional deep mantle tomography inversion that included 3D kernels. The addition of extra ray paths for waves triplicated by the discontinuity enhances resolution of the radial structure, as differential times between the D″ reflector and the CMB reflection (ScS) provide sensitivity to radial structure not achieved by the path-integral anomalies for ScS (or ScS-S differential anomalies) alone (**Figure 3**). There are technical issues involved in seismic tomography when the ray path is particularly sensitive to the model perturbations, as is the case for grazing triplication phases, but this example demonstrates that conventional seismic tomography using major phases alone is not likely to resolve fine-scale deep mantle structure. Extracting more information than just phase arrival times from seismic waves that traverse the deep mantle involves either waveform modeling or wavefield imaging approaches, or some combination of both. For the remainder of this review, we focus on waveform-based methods that are sensitive to and can retrieve the fine-scale structure.

WAVEFORM MODELING METHODS

Waveform modeling involves comparison of synthetic ground-motion predictions with observations. Model velocities are adjusted to yield synthetic seismograms that match the arrival times and amplitudes of primary waves as well as secondary arrivals produced by reflections, triplications, multipathing, and diffraction. As P- and S-wave wavefronts interact with the spherical CMB at grazing distances, the amplitudes of major phases reflected or transmitted at the CMB (**Figure 1**) such as PcP, PKP, PKKP, PcS, ScP, ScS, SKS, SKKS, and SPdiffKS become increasingly sensitive to the velocity gradients and contrasts in the deep mantle. Some studies utilize top-side core reflections at close-in epicentral distances (<∼60°) where wavefield interactions with the CMB are precritical and where both primary and secondary arrivals are very small and mainly sensitive to impedance contrasts across the CMB or other deep mantle structures. However, most studies are conducted at epicentral distances greater than ∼70°, which is the domain of near- and postcritical angles of incidence. Even small velocity gradients or discontinuities can then produce relatively large secondary arrivals linked to the each of the major phases. When such secondary arrivals are directly observed in individual signals or when they are enhanced through summing multiple aligned signals (stacking) with similar paths, it becomes possible to perform iterative or inverse waveform modeling, which adds velocity gradients and discontinuities to smooth reference Earth model structures.

Typical SH-wave seismogram profiles beyond 70° epicentral distance for deep focus earthquakes are shown in **Figure 4**. In this range, a simple Earth model such as PREM predicts that only major phases S and ScS should be observed and that their absolute and differential arrival times can be used for tomography, whereas their amplitude ratios and waveshapes can be modeled to constrain velocity gradients above the CMB (e.g., Lay & Helmberger 1983b, Ritsema et al. 1997). The waveform profiles also show other ground motions, some of which constitute ambient noise that is incoherent from station to station (like that preceding S) and some of which have systematic move-out relative to S and ScS as the epicentral distance increases (like the phase labeled Scd). Such an extra phase, readily visible in individual traces at these wide-angle distances, is a candidate for direct waveform modeling or for waveform stacking and migration methods. There may be additional low-amplitude arrivals that are not apparent in the individual waveforms because they have signal-to-noise ratios less than 1; signal enhancement procedures are needed before any such arrivals can be detected and modeled.

The Scd phase in **Figure 4** was first forward modeled as a triplication from a 2.5–3% S-wave discontinuity 250–300 km above the CMB by Lay & Helmberger (1983a), and, together with a few instances of comparably visible P-wave reflected (PdP) arrivals, has been the subject of many subsequent direct modeling efforts (see Lay & Garnero 2007 for a review). The typical strategies have been to forward-model distance profiles of observations in a process that exploits the differential move-out of the different arrivals to constrain the depth and velocity contrast across the discontinuity, or to model individual waveforms where differences in the coda of S compared with the coda in ScS are used to identify the Scd arrival. These approaches are viable because of the large amplitude of PdP and Scd in some profiles, but resulting models are potentially biased toward regions with particularly strong D″ discontinuities and are subject to uncertainties in the forward-modeling parameter space (e.g., Thorne et al. 2007).

A waveform inversion approach for S waves that graze the CMB and that may not have such clearly identifiable waveform complexities in individual traces has recently been developed by Kawai et al. (2007a) and Kawai & Geller (2010). This method, although potentially extendable to 3D inversion, has been used to obtain 1D structures by inverting dense sets of observations, typically from distances greater than 80°, and sampling localized regions of the lowermost

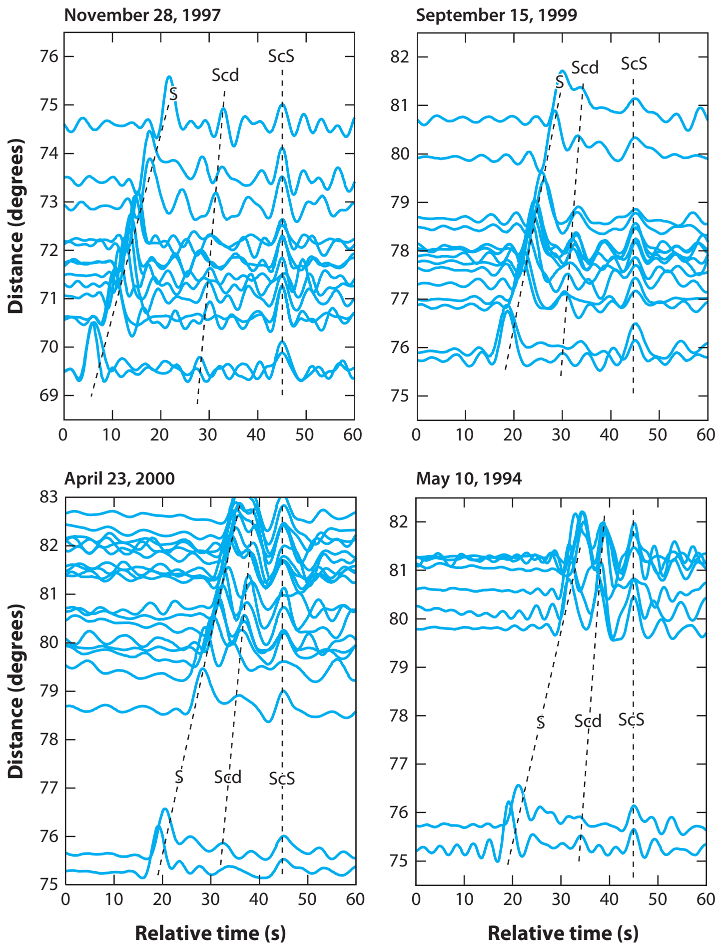

Figure 4

Distance profiles of broadband tangential- (SH-) component ground displacements that have been source equalized by deconvolution of a reference wavelet from the aligned and stacked ScS phases for each event (from Thomas et al. 2004a). The traces are aligned on the peak of ScS at an arbitrary time of 45 s. The first arrival is direct S, which turns in the mid-mantle. Between S and ScS are other arrivals including noise; signal-generated reverberations unique to each station; and a consistent arrival, Scd, that has systematic arrival-time move-out relative to S and ScS, indicating that it is a deep mantle reflection/triplication phase. This type of phase can be waveform modeled, stacked, and migrated.

mantle. The method uses complete synthetic waveforms and their partial derivatives relative to a spherical (or aspherical) model. Numerous waveforms can be used, and even if secondary arrivals are smaller than those shown in **Figure 4**, a localized 1D model can be extracted by a formal waveform-matching criterion analogous to surface-wave waveform inversion approaches that extract structure from strongly interfering wave reverberations. This has the attraction of an objective measure of model fit, although the nonlinear nature of the waveform inversion allows inversion variance to be strongly affected by unmodeled 3D variations that can potentially bias the 1D solution. This approach has been applied in areas in which earlier forward-modeling efforts have established the existence of good path coverage, such as beneath the Arctic (Kawai et al. 2007a), northern Asia (Kawai et al. 2009), Central America (Kawai et al. 2007b), the western Pacific

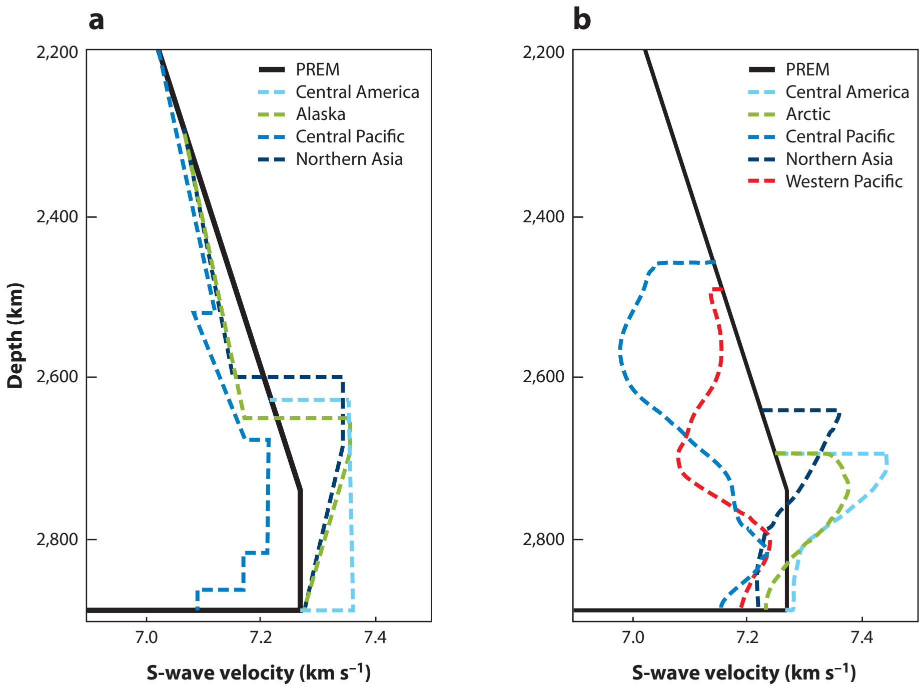

Figure 5

Comparison of 1D S-wave models obtained for various localized regions of the lowermost mantle (*a*) by forward modeling of data profiles or stacks and (*b*) by waveform inversion. (*a*) Central America, Lay et al. (2004a); Alaska, Young & Lay (1990); central Pacific, Ohta et al. (2008); northern Asia, Gaherty & Lay (1992). (*b*) Central America, Kawai et al. (2007b); Arctic, Kawai et al. (2007a); central Pacific, Kawai & Geller (2010); northern Asia, Kawai et al. (2009); western Pacific, Konishi et al. (2009). In all cases, the sharp velocity increases could be distributed over 30–50 km in depth given the limited resolution of the data, and there are uncertainties in absolute velocities owing to the choice of Preliminary Reference Earth Model (PREM) as a reference model. All models must involve some lateral averaging over the sampled domain.

(Konishi et al. 2009), and the central Pacific (Kawai & Geller 2010); thus this approach effectively provides an independent determination of the structures that is distinct from forward-modeling approaches. The localized 1D models from waveform inversion (relative to a smooth PREM-like starting model or one with a first-order discontinuity at a specified depth) tend to share basic features inferred from forward-modeling approaches (**Figure 5**). The most notable among these features are relatively strong S-wave velocity increases at depths from 200 to 300 km above the CMB, which give rise to the Scd triplication, and a velocity reduction in the lowermost 100 km of the mantle. Most applications to date have rather limited radial resolution and cannot distinguish between a sharp velocity discontinuity and a velocity gradient distributed over ~100 km in depth extent. Forward modeling has similar limits on resolution, although use of carefully processed higher-frequency data can improve resolution of viable velocity gradients, as discussed below.

Forward modeling of waveforms has continued to play a major role in constraining lateral gradients in deep structures, particularly those associated with the margins of Large Low Shear wave Velocity Provinces (LLSVPs) in the deep mantle beneath the south-central Pacific and Africa-southern Atlantic-southern Indian Ocean regions that were initially partially imaged by global mantle tomography (Helmberger et al. 2000). Wen et al. (2001) used 2D waveform synthetics from a hybrid finite-difference/ray-theory method (Wen 2002) to model wide-angle SH signals traversing a steeply dipping western margin of the LLSVP beneath Africa. They modeled the data with 300-km-thick zones of low (-2% to -12%) shear velocity above the CMB over an extensive area. Wen (2001) obtained a similar, 200-km-thick structure for the eastern margin of the LLSVP below the southern Indian Ocean sampled by SKS, S, and ScS paths. Wang & Wen (2004) further mapped the configuration of the low-velocity province, proposing that it has an L-shaped form that changes from a north–south orientation under the south Atlantic to an east–west orientation under the southern Indian Ocean and that it features a total volume of $\sim 4.9 \times 10^9$ km^3. Ni et al. (2002) used SKS phases to straddle the margins of the African anomaly and used sharpened velocity gradients in tomography models to match travel time, amplitude, and waveform variations across the margins. They used a modified ray-theory method (Ni et al. 2000) to calculate synthetics for 2D profiles through tomography models, which have low velocities extending up from the CMB much higher into the lower mantle than the 300 km proposed by Wen and coworkers. They found sharp lateral boundaries of the LLSVP, with average velocity reductions of $\sim 3\%$ between "normal" mantle and LLSVP material. Further 2D waveform and travel time modeling efforts by Ni & Helmberger (2003a,b) using increased ray-path coverage with S, ScS, and SKS arrivals from portable station deployments in Tanzania and South Africa support the case for the LLSVP extending up to $\sim$1,200 km above the CMB beneath Africa; the southern Pacific LLSVP may not extend as far up into the lower mantle. Spectral-element modeling and approximate generalized-ray-theory 3D modeling confirmed that the southeastern margins of the African LLSVP involve lateral gradients of 3% in S-wave velocity over distances of $\sim$100 km or less (Ni et al. 2005). The differences in the models from the two groups demonstrate a typical trade-off in forward modeling between the thickness of a zone that contains anomalous velocities and the amplitude of the velocity perturbation. The differences in models of the African LLSVP were largely reconciled by an expanded data set of S, ScS, SKS, and SKKS that was subsequently analyzed by Wang & Wen (2007), who confirmed an upward extension of the reduced velocities (**Figure 6**).

Smaller-scale structural features have been recently put forth. For example, D. Sun et al. (2007) examined waveform details to detect internal structure within the African LLSVP. Sun et al. (2009) developed a multiple-arrival detector that allows waveform complexity to be related to lateral gradients in structure, which can then be modeled through the use of 3D synthetics. This exploits the common observation of a fast arrival that travels through higher-velocity material and a secondary arrival that travels through adjacent lower-velocity material. Tomographic models are used to guide the modeling process, as described by Helmberger & Ni (2005). Sun et al. (2010) used the multipath detector to model a localized waveform complexity attributed to a narrow plume extending upward from the LLSVP, suggestive of a boundary layer detachment from a large chemical anomaly.

Similar waveform modeling efforts have been applied to circum-Pacific regions of D″. Garnero & Lay (2003) combined travel time, shear wave splitting, and triplication-arrival detections to explore the deep structure beneath the Caribbean and Central America, confirming widespread occurrence of an S-wave reflector plausibly associated with the top of D″. Strong lateral gradients in PKP travel times and waveforms across the region indicate a sharp western edge to the high-velocity region beneath the Cocos plate (X. Sun et al. 2007). Sun et al. (2006) modeled waveforms sampling D″ beneath Central America, enhancing tomographic structure by adding a discontinuity and modeling triplication arrivals that they attributed to a phase transition in folded slab material. Sun & Helmberger (2008) extended the strategy of Sidorin et al. (1999), involving a parameterized phase-transition boundary that enhances radial gradients in tomographic models used to model S-wave profiles in localized regions beneath the eastern Pacific, Mexico, and northern South

America. They found that the height of the D″ transition above the CMB varies from 100 to 240 km and that the velocity jump at the transition varies from 1% to 4%. A phase transition Clapeyron slope of 9 Mpa K^{-1} is preferred for matching the variations. Wallace & Thomas (2005) found comparable relief on the D″ reflector that varies between 86 and 286 km above the CMB under the north Atlantic by waveform modeling of S waves at distances of 85 to 93°, which are beyond the expected triplication cross-over distance for a lower-mantle discontinuity.

Structure of the LLSVP beneath the Pacific has also been the target of waveform modeling studies. He et al. (2006) used S and ScS travel time observations and waveform modeling for numerous paths traversing the northwestern boundary of the LLSVP that extends northeastward

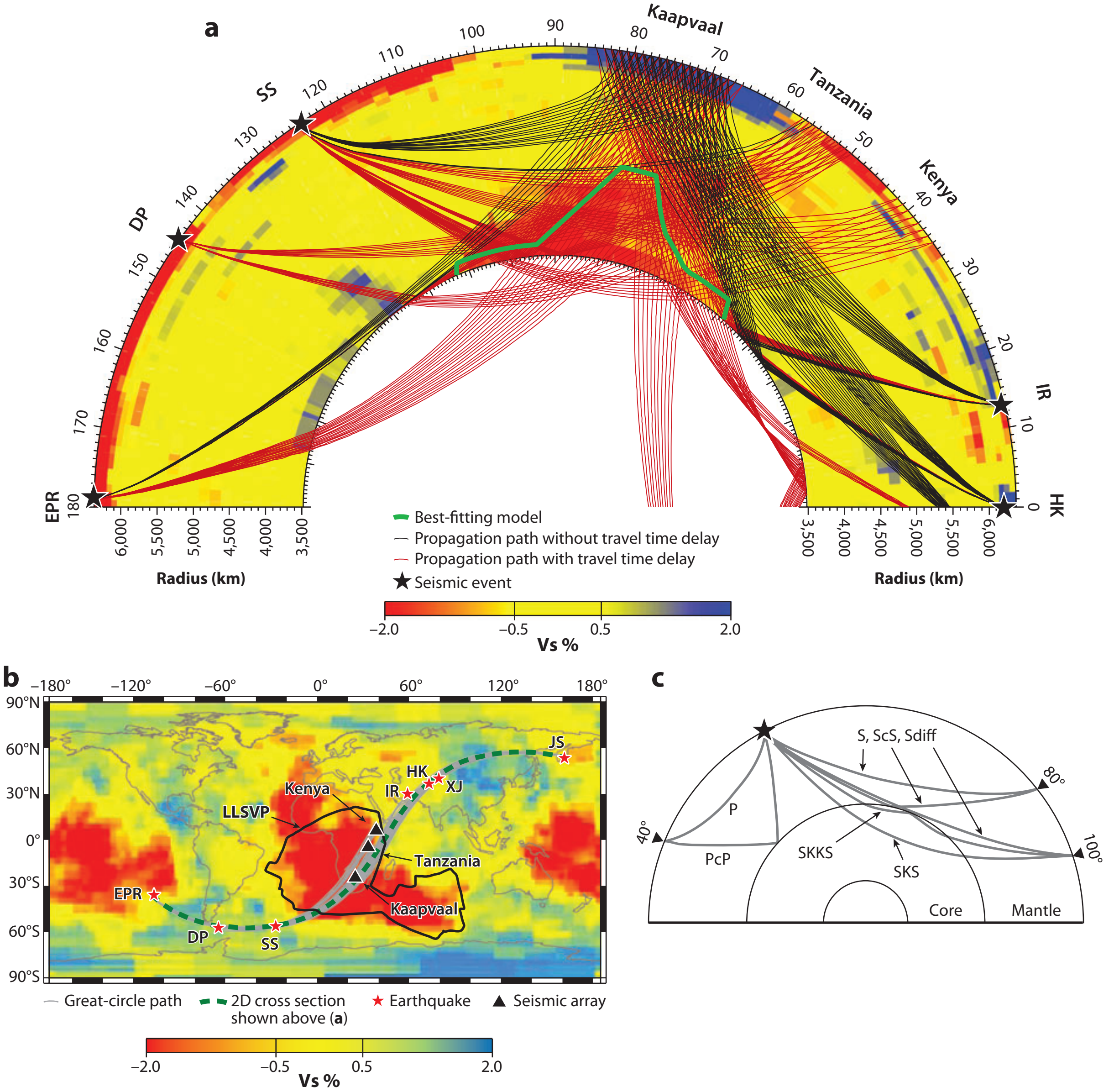

from New Guinea, finding an average S-wave velocity reduction of −5% in the lowermost 300 km. On the outer margin of the LLSVP, they detected an abrupt 2% velocity increase 100–145 km above the CMB, an area that features a 30-km-thick basal layer with a −13% reduction near the edge of the region. However, He et al. (2006) found no discontinuity with more than a −2% reduction in the central region of the LLSVP. The western edge of the LLSVP is quite abrupt, and this is supported by differential time analysis by Takeuchi et al. (2008), who argued for a 4% velocity change over ∼200 km laterally based on ScS-S and sScS-sS differential time patterns for a zone extending upward 400 km from the CMB. He & Wen (2009) extended the analysis of the Pacific LLSVP using SKS, SKKS, and Sdiff arrivals, including paths sampling the southeastern margin of the structure. They found evidence for the LLSVP having two separate regions of low velocity with a 740-km-wide gap between them. The western portion extends upward 740 km from the CMB, and the eastern portion reaches at least 340 km above the CMB. Tomography models are used to correct travel times on portions of the paths outside the LLSVP, which is a potential source of error, but spatial gradients in times and differential times between phases do constrain the margins of the LLSVP structure where there is dense wave-path coverage. Strong lateral velocity gradients at the southern and southeastern LLSVP margins are found by azimuthal patterns in waveform complexity by To et al. (2005) and Ford et al. (2006). They found that the main effect, again, is the arrival of a slow phase that travels within low-velocity LLSVP material following an earlier phase that travels in external high-velocity material. Lateral variations in PKPab travel times and multipathing also indicate strong lateral gradients at the northern end of the Pacific LLSVP (Luo et al. 2001).

Waveform modeling has played a central role in investigations of the ultralow-velocity zones (ULVZs) directly above the CMB. In this case, the primary phases are PcP, ScP, ScS, and SPdiffKS, all of which involve reflections or diffractions at the CMB and additional phases generated by reflections and conversions from nearby strong velocity gradients on either the mantle or core side. Waveform and limited array analysis of SPdiffKS, the phase generated by the critical angle for conversion of S to P energy at the CMB on both the source and receiver sides of the SKS path, provide broad sampling of the ULVZ (Stutzmann et al. 2000, Rondenay & Fischer 2003, Thorne & Garnero 2004, Thorne et al. 2004, Rondenay et al. 2010). It remains challenging to partition structural effects between the source and receiver sides of the ray paths. More localized and shorter-period signal analysis has added detail to ULVZ models through the modeling of P-wave and ScP data profiles and linear stacks (Garnero & Vidale 1999; Castle et al. 2000; Reasoner & Revenaugh 2000; Persch et al. 2001; Castle & van der Hilst 2003; Rost & Revenaugh 2003;

Figure 6

(*a*) Best-fitting model (*green contour*) and ray paths of the seismic phases employed to constrain geometry and S-wave velocity structure of the African Large Low Shear wave Velocity Province (LLSVP) in a 2D cross section along the East Pacific Rise (EPR), Drake Passage (DP), South Sandwich islands (SS), Iran (IR), and Hindu Kush (HK). Black and red traces represent propagation paths without and with observed travel time delays that can be attributed to the African LLSVP, respectively. The geometry of the African LLSVP is confined below the paths with no travel time delays (*black traces*). The best-fitting model has average reductions of −5% in shear velocity and −1.67% in compressional wave velocity in the lowermost 250 km of the mantle and sharp velocity drops of −2% to −3% in shear velocity and approximately −1% in compressional wave velocity 150–250 km above the core-mantle boundary (CMB). Black stars represent seismic events. Seismic arrays and earthquake locations are denoted at the top of Earth's surface. The background colors are S-wave velocity perturbations from a global shear velocity (Vs) tomographic model (Grand 2002). (*b*) Map view of great-circle paths (*gray traces*), locations of earthquakes (*red stars*), and seismic arrays (*black triangles*). The thick green dashed curve represents the 2D cross section represented in panel *a*, and the thick black contour is the geographic boundary of the LLSVP at the base of the mantle. The collected seismic data sample the African anomaly in a narrow azimuthal range of less than 11°. Abbreviations: JS, Japan Sea; XJ, Xinjiang China. (*c*) Ray paths of direct S; ScS at 80°; P; PcP at 40°; and Sdiff, SKS, and SKKS at 100°. From Wang & Wen (2007).

Rost et al. 2005, 2006; Garnero et al. 2007b; Idehara et al. 2007; Xu & Koper 2009; McNamara et al. 2010; Rost et al. 2010a,b). These studies support earlier work that found strong velocity reductions for P-wave and S-wave velocities intermittently in piles or thin (10–30 km-thick) layers right above the CMB with horizontal scale lengths of ∼50 km to >1,000 km. Waveform modeling sensitivity studies indicate some ambiguity in whether the anomalous structure is concentrated (*a*) on the mantle side of the CMB or (*b*) in a thin zone of finite rigidity or anomalous P-wave velocity on the core side (Buffett et al. 2000, Garnero & Jeanloz 2000, Rost & Revenaugh 2001). Given the subtle precursors and postcursors generated by layering near the CMB, 1D waveform modeling of ULVZ structure must be practiced judiciously, as lateral variations can produce complex arrivals. Small aperture arrays with short-period instrument response prove particularly valuable for these studies.

Waveform modeling methods are also intrinsic to quantification of the waveform stacking and migration approaches for waves with varying slownesses and azimuths (see below). Although many applications using localized 1D modeling procedures are viable, 2D, 2.5D, and 3D methods are increasingly applied to address the deep mantle imaging problem. The presence of strong heterogeneity with complex configurations is clearly indicated by seismic observations, and this motivates more flexible migration imaging rather than forward-modeling or 1D waveform inversion approaches, although the long path lengths of the data that sample the region and the limited bandwidth still intrinsically pose many difficulties for resolving deep structure.

SLOWNESS AND AZIMUTHAL STACKING PROCEDURES

The waveform modeling approaches described above rely mainly on matching with synthetic seismograms specific waveform features in individual seismograms, in distance profiles of observations, or in linear stacks of individual phases; thus they depend on having relatively strong isolated arrivals. However, precritical reflections and triplications from small velocity changes anywhere in the medium may be at or below the background noise level, and modeling is possible only if the signals are first detected by stacking multiple signals over a distribution of possible scattering locations. This involves summing time-shifted signals from different stations as a function of either distance or azimuth, and finding the preferred slowness (inverse apparent velocity) and/or azimuth that best enhances secondary arrivals and allows them to be associated with particular paths in the lower mantle. Some studies apply such methods as detection procedures (e.g., Kito et al. 2007b), whereas others compute synthetic seismograms for velocity models and process them similarly to how they process the data attempting to match the observed slowness and azimuthal behavior (e.g., Hutko et al. 2008). Thus the latter type of study merges imaging and modeling approaches.

The travel time (T) curves as a function of epicentral distance (Δ) for seismic phases in a 1D Earth model (**Figure 1**) have distinct slopes (dT/dΔ; also known as the seismic ray parameter or slowness) that vary smoothly with distance. Measuring the arrival time and slowness of a given phase indicates the nature of the phase and the depth/velocity at which it turns in Earth. This holds both for major phases in a reference model and for any additional phases triplicated or scattered by strong velocity gradients in Earth. A standard way to search for additional phases is to align and sum seismic recordings from a seismic array or small network, varying the relative timing to account for a range of possible phase slownesses and statistically evaluating the summed signal energy to detect arrivals. Many such methods have been introduced (Rost & Thomas 2002). **Figure 7** shows a slowness stack as a function of time (vespagram) for S waves recorded by broadband Transportable Array stations in North America for an intermediate depth event in the deep Japan slab. The main S and ScS phases and their associated depth phases (sS and sScS) are observed at the expected slownesses for a standard Earth model, and intermediate slowness arrivals (Scd and

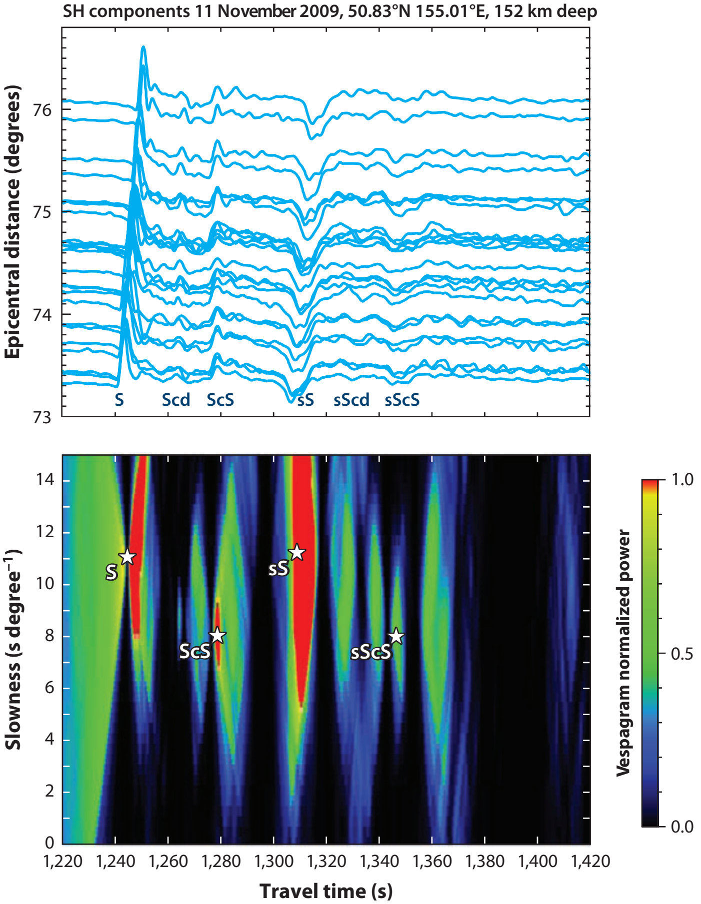

Figure 7

Example of a transverse-component data profile (*top*) and normalized seismogram-stack power for varying slowness versus time (vespagram, *bottom*) for SH waves recorded by the Transportable Array for intermediate-depth earthquakes. The major phases seen in the seismograms (S, ScS, sS, sScS) produce clear peaks in vespagram power (*stars*) with corresponding slownesses for a simple reference Earth model such as Preliminary Reference Earth Model (PREM). An extra arrival with intermediate slowness and variable strength is identified between S and ScS as Scd, the triplication phase from a lower-mantle shear velocity increase ~250 km above the core-mantle boundary (CMB). Energy is also seen between sS and sScS, consistent with a lower-mantle reflection (i.e., sScd).

sScd, like those shown in **Figure 4**) are apparent between the main arrivals. Vespagram processing establishes the presence of seismic energy not predicted by a standard model and indicates its slowness, and the stacking suppresses effects of incoherent noise to avoid misidentifying signals generated at the receivers. One would expect that a single station would record Scd arrivals with similar slowness for a suite of similar sources that span a range of distances (Lay & Helmberger 1983a). Stacking the seismograms as a function of azimuth from the receivers can also be done to evaluate whether any extra arrival is in the great-circle plane with the main phases or is scattered from out of plane, and whether strong lateral gradients in seismic velocity are present.

Combining stacks of data for multiple events and multiple stations is the most extensively practiced approach for deep mantle imaging. Krüger et al. (1993) introduced a double-array method for arrays of sources and receivers in which signals are shifted and stacked for possible scattering positions in the medium. They applied it to P waves to detect or demonstrate the absence of deep mantle reflectors under Eurasia and the Arctic (Krüger et al. 1995, 1996; Weber et al. 1996). A similar procedure for double-array stacking in common reflection-point bins that are distributed at varying depths above the CMB was introduced by Yamada & Nakanishi (1996), and this method was applied to detect P-wave reflectors 170–270 km above the CMB in the deep mantle under the southwest Pacific (Yamada & Nakanishi 1998). The same basic strategy was incorporated into double-beam imaging by Scherbaum et al. (1997) and Kaneshima & Helffrich (1998), in methods that seek to detect any single forward-scattering arrivals in stacks of seismic energy (beams) as functions of travel time, slowness, and azimuth. These methods allow the combination of many signals to evaluate the structure in a localized reflection-point region. Kito & Krüger (2001) analyzed seven deep Fiji events recorded at the J-Array in Japan, applying an extension of double-beam imaging that integrates source-array beam forming with receiver-array beam forming in a simplified form of migration. They applied the process using a 3D grid with 50-km spacing from 2,950 to 2,500 km, inferring reflections from two velocity decreases near 2,550- and 2,650-km depth with amplitudes constituting a very small fraction of that of the core-reflection PcP. This result conflicts with those of Yamada & Nakanishi (1998) for the same area. Given strong wavefield scattering in the D″ region in many places (Garnero 2000), it is unclear whether local 1D model interpretations of weak features are valid.

Equalizing the source signal is important for coherent stacking of signals from different earthquakes. This can be achieved by stacking signals on manual alignments or on a predicted move-out for a reference phase, and then deconvolving the stacked wavelet from the signals to extend the bandwidth, effectively "spiking up" the residual waveforms relative to the original signals (e.g., Revenaugh & Meyer 1997, Kito & Krüger 2001). This usually requires application of a low-pass filter but equalizes the bandwidth and signal shape, improving coherency of signals from different events (**Figure 4** shows examples). Weighting the individual signals and the event stacks can be done on the basis of various criteria. Kito & Krüger (2001) performed phase-weighted stacking using semblance (Schimmel & Paulssen 1997). Semblance is an amplitude-dependent measure of coherency among the aligned signals that are summed in a beam. Gaussian functions were also applied to weight the signal intervals around the predicted time for a given stacking target location. These weighting strategies are usually nonlinear and may provide overly optimistic apparent resolution of the structure.

Thomas et al. (2002) used P-wave vespagrams and frequency-wavenumber stacks as functions of slowness (with Nth-root stacking) and backazimuth to study the deep mantle under the northern Pacific using P waves from northwestern Pacific earthquakes recorded at Yellowknife, Canada. They detected PdP reflections from a discontinuity varying from 211 to 336 km above the CMB, with only a few degrees of variation in backazimuth relative to the direct P wave. Braña & Helffrich (2004) used slowness versus travel time and slowness versus azimuth stacks to seek P reflections from D″ for Mexico earthquakes recorded at an array in the United Kingdom. They applied a joint likelihood of scattering calculation as a probabilistic measure of the stacked energy over a grid (Kaneshima & Helffrich 1998) for each earthquake, and they multiplied the probabilities together for multiple events. A 700-km-scale, high-velocity scattering region was detected near 2,720-km depth under Nova Scotia.

Reflections from structure just above the CMB and near the top of D″ have been the subject of many double-array-stacking applications. Using short-period regional seismic network data, Revenaugh & Meyer (1997) found evidence for strong P-wave velocity reductions in thin layers (ULVZs) in several regions in double-array stacks. Applying double-array stacking to a range of common reflection target depths is a limited form of migration that assumes that any coherent reflected energy is a precritical reflection from in-plane structure over some averaging bin scale length. Using double-array stacks of regional short-period network data, Reasoner & Revenaugh (1999) identified P-wave reflectors from the top of D″ under the central Pacific and Central America. These regions were subsequently studied further through the use of double-array stacks of P and SH data by Castle & van der Hilst (2000), Havens & Revenaugh (2001), Russell et al. (2001), Lay et al. (2004a), Flores & Lay 2005, Avants et al. (2006a,b), Lay et al. (2006), Hutko et al. (2008, 2009), Lay (2008), and Ohta et al. (2008). These double-array-stacking studies combine 1D data stacking with similar treatment of synthetic seismograms for localized 1D velocity models, accounting for the complete effects of triplications on near-critical P- and S-wave signals interacting with deep discontinuities. Both data and synthetics are stacked for horizontal bins containing nearby reflection points, seeking precritical reflections from various target depths in a reference velocity model (which has no actual velocity contrasts at those depths). Therefore, phase shifts of both postcritical reflections and turning waves in triplications are accounted for, but they project to artificial reflector depths. Effects of inaccurate reference velocity structure are hard to quantify but can be constrained by performing double-array stacking relative to alignments on different reference phases (such as P or PcP and S or ScS). Seeking models that fit the data stacks for varying reference phases suppresses but does not fully eliminate the effects of biases in the reference structure (e.g., Lay et al. 2006, Lay 2008).

As ever larger data sets have been analyzed, multiple velocity features have been introduced in the local 1D models, as demonstrated for the region below the Cocos plate studied by Hutko et al. (2008) (**Figure 8**) and Lay (2008) (**Figure 9**). By deconvolving source wavelets and stacking hundreds to thousands of signals in localized common reflection-point bins, weak arrivals such as PcP are stably recovered and can be aligned for use as a reference phase for detecting even weaker features. [This leads to models that have abrupt discontinuities involving velocity contrasts as small as 0.1% for P waves (**Figure 8**) and S waves (**Figure 9**).] In this circum-Pacific region, the P-wave reflections from D″ are small and appear to indicate a small P-wave velocity decrease in contrast to a ∼2% S-wave velocity increase at the same depth, but in other areas stronger P-wave reflections are observed (see Lay & Garnero 2007). The double-array-stacking approach is limited to localized 1D processing, but separate stacking in spatially offset common reflection-point bins allows lateral variations to be detected. An example is shown in **Figure 10**, from Lay et al. (2006), for S-wave velocity structure under the central Pacific. Here, several reflectors are inferred from modeling the data stacks for adjacent bins, and these show systematic variations in depths of reflectors. Using 1D modeling of very small apparent reflectors in the presence of strong lateral 2D or 3D heterogeneity is obviously questionable, as is extrapolating between the adjacent structures (Thorne et al. 2007). This motivates more complete imaging of the structure through the use of full 3D migration methods.

MIGRATION METHODS

The essence of seismic migration is similar to the double-beam approaches described above: Wave energy is tracked down from multiple sources and from multiple stations to a 3D configuration of target grid locations in the lower mantle through the use of ray tracing in an Earth reference structure. Seismograms are shifted to correspond to predicted arrival times for each grid point and then stacked with various filters and weighting schemes to determine whether any coherent seismic reflection from that grid location is evident. Seismic migration in shallow exploration seismology emphasizes wavefield reconstruction and downward wave propagation. In doing so, it usually applies geometric spreading and sometimes attenuation corrections such that the migrated image is directly related by a specific imaging criterion to material property contrasts in the medium

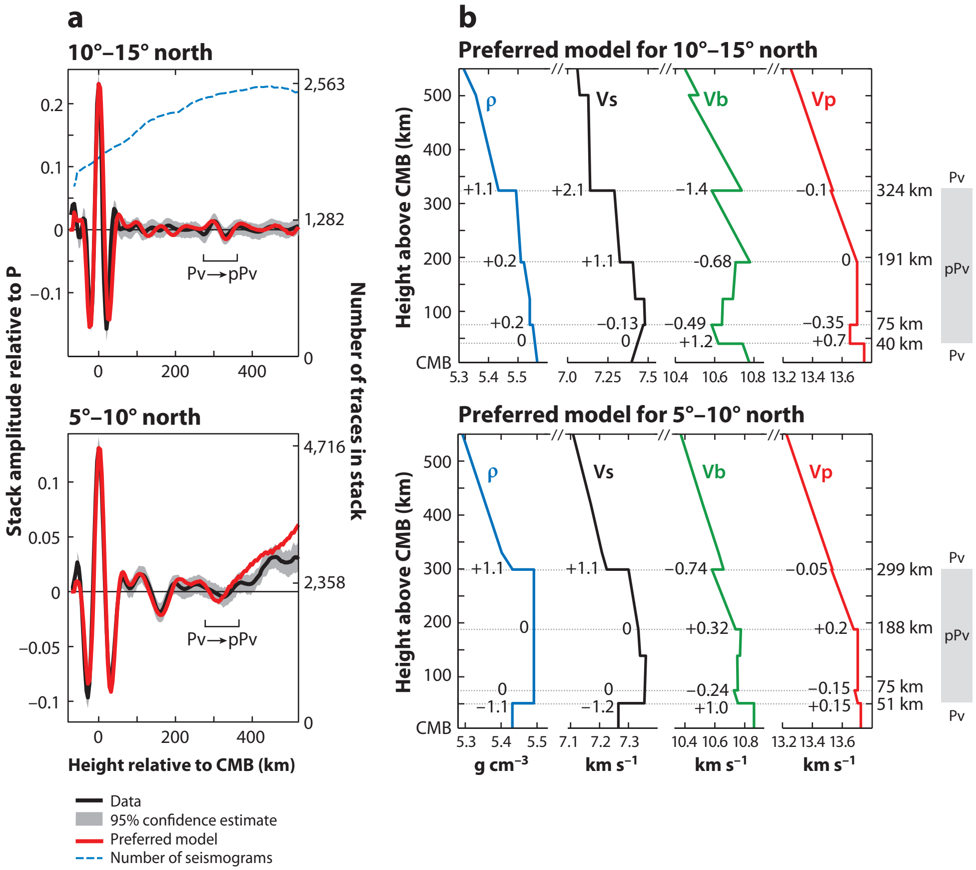

Figure 8

Examples of double-array stacks of P waves recorded in Southern California with paths that sample the deep mantle beneath the Cocos plate, west of Central America. (*a*) The data stacks (*black traces with gray 95% confidence estimates*) are aligned on PcP with amplitudes relative to direct P. Synthetics for the corresponding path-receiver geometries identically processed are shown in red. (*b*) The corresponding velocity (Vs, S-wave velocity; Vb, bulk-sound velocity; Vp, P-wave velocity) and density (ρ) profiles. The S-wave velocities were independently determined (see **Figure 9**), and very small features in the P-wave structure are inferred from the high-quality data stacks. CMB, core-mantle boundary. The depths of velocity discontinuities and the estimated depth extent of perovskite (Pv) and post-perovskite (pPv) are indicated on the right. From Hutko et al. (2008).

(often impedance or acoustic velocity contrasts). Most applications of migration methods for deep Earth investigations are less formal; because the first-order problem has been to detect coherent secondary arrivals, amplitudes are commonly defined relative to some reference phase, which has its own geometric spreading and attenuation effects. Shallow migrations largely involve precritical angles of interaction with quasi-horizontal structures and rely on multiple sampling of the structure with varying angles to characterize the reflectors. For deep mantle applications, the limitations on slowness and azimuthal sampling of any given deep region degrades the resolution of stacking and migration methods, and results differ in the way that artifacts are suppressed.

Early deep mantle migration approaches focused on the kinematic constraints provided by arrays of sources and receivers to define possible scattering locations based on intersections of

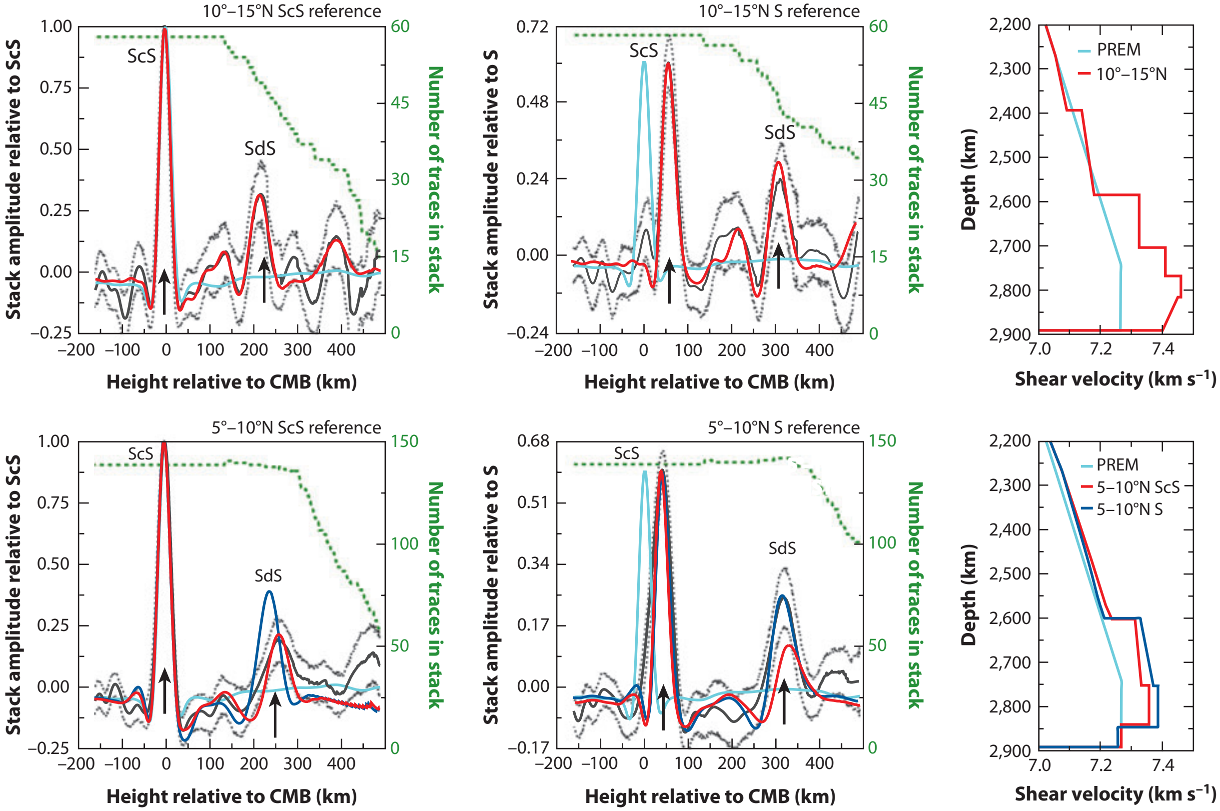

Figure 9

Double-array stacks of SH-wave data (*left*, *middle*) bottoming in the lowermost mantle beneath the Cocos plate (*solid gray lines with dotted lines indicating 95% confidence estimates in the stacks*) compared with stacks of synthetics for the color-coded velocity models (*right*). The number of traces in the stack at each depth is indicated by the green dashed curves and the scales on the right of each panel. In the left column, the data were prealigned and amplitude normalized on the readily observed core-reflection ScS, whereas stacks aligned on the S phase are shown in the middle. Abrupt velocity increases near 2,600 km give rise to the SdS feature (a combination of Scd and the postcritical reflection Sbc) in the stacks, and smaller secondary features are modeled to give additional velocity increases and decreases. Shifts of the average lower-mantle velocity structure shallower than 2,600 km deep relative to Preliminary Reference Earth Model (PREM) are indicated by the misfit of PREM synthetics for the stacks relative to S. CMB, core-mantle boundary. From Lay (2008).

isochronal (constant–travel time) surfaces (Lay & Young 1996, Bilek & Lay 1998). These methods used simple spike-train approximations (involving a series of impulsive arrivals with relative times and amplitudes) deconvolved from long-period SH waves and established the likelihood that Scd arrivals for paths beneath Alaska and Eurasia are indeed generated from near the top of D″ rather than from mid-mantle scattering locations. Freybourger et al. (2001) used complete P-wave recordings to migrate for D″ structure under the Arctic, motivated by variability in double-array stacks and out-of-plane scattering of PdP phases in the region. The basic assumption in the migration is that the wavefield generated at a given grid point is an isotropic point scatterer, which allows data from varying ranges to be linearly combined in a stack. Kito & Krüger (2001) applied double-array beam forming of P waves over continuous grids, complementing their phase-weighted-semblance, double-array-stacking method. This was further applied by Kito et al. (2004) to P waves and S waves sampling the lowermost mantle beneath the southwestern Pacific, and the study inferred reflections from velocity decreases with depth based on comparisons with

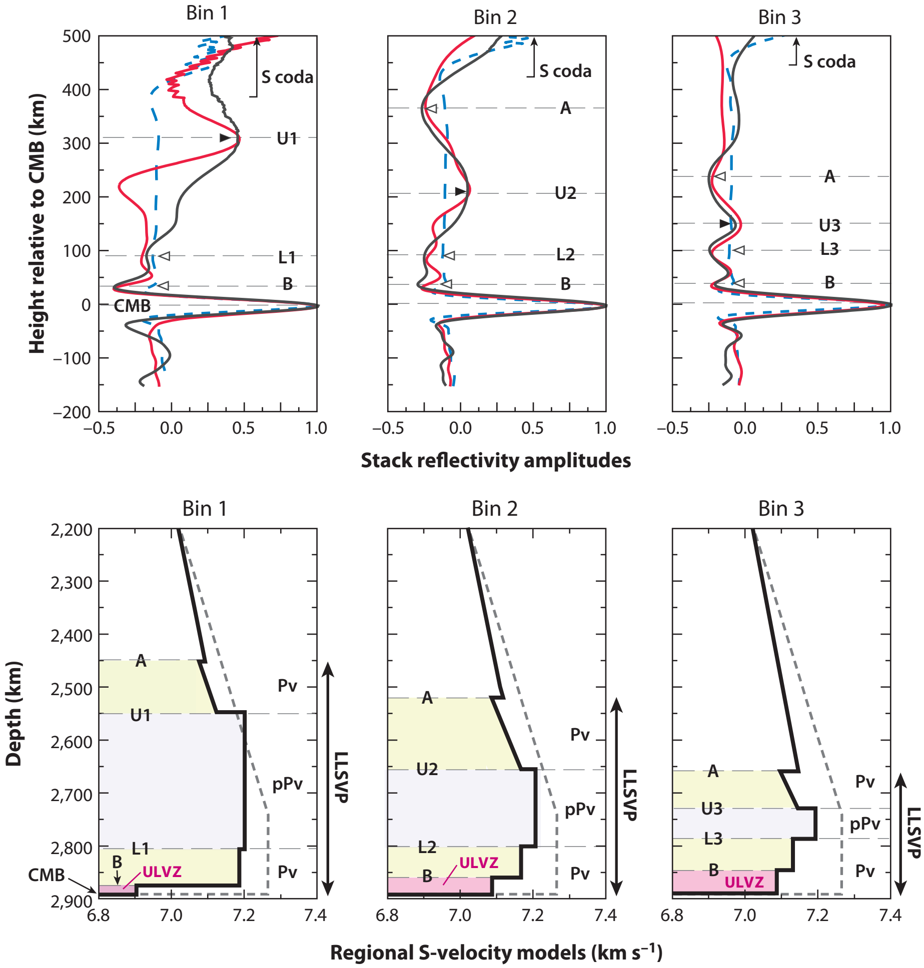

Figure 10

Double-array stacks of S waves that sample the lowermost mantle under the central Pacific (*top row*, *gray curves*) compared with stacks of synthetics for Preliminary Reference Earth Model (PREM) (*dashed blue traces*) and for the velocity models shown in the bottom row (*red traces*). The three bins are adjacent to one another from southwest (Bin 1) to northeast (Bin 3), and the differences in the localized stacks indicate strong lateral variations in the structure. The velocity models show systematic variations of common features, with the U discontinuity deepening toward the northeast while the L discontinuity shallows. This likely corresponds to a thinning lens of postperovskite (pPv) sandwiched between layers of perovskite (Pv) near the northeastern margin of the Pacific Large Low Shear wave Velocity Province (LLSVP). A velocity decrease (A) may correspond to the upper boundary of the LLSVP. Another velocity decrease (B) at the top of a laterally varying ultralow-velocity zone (ULVZ) is also present. CMB, core-mantle boundary. From Lay et al. (2006).

similarly processed synthetics. Chaloner et al. (2009) studied the seismically high-velocity areas beneath southeastern Asia using earthquakes from the South Pacific region recorded by permanent and portable networks in central Asia. They applied several array methods and point-scattering migrations to P and S waves, finding consistent reflector depths for both wave types with a negative impedance contrast for P and a positive impedance contrast for S. There is some evidence for a second, deeper reflector beneath the northeastern end of the study region.

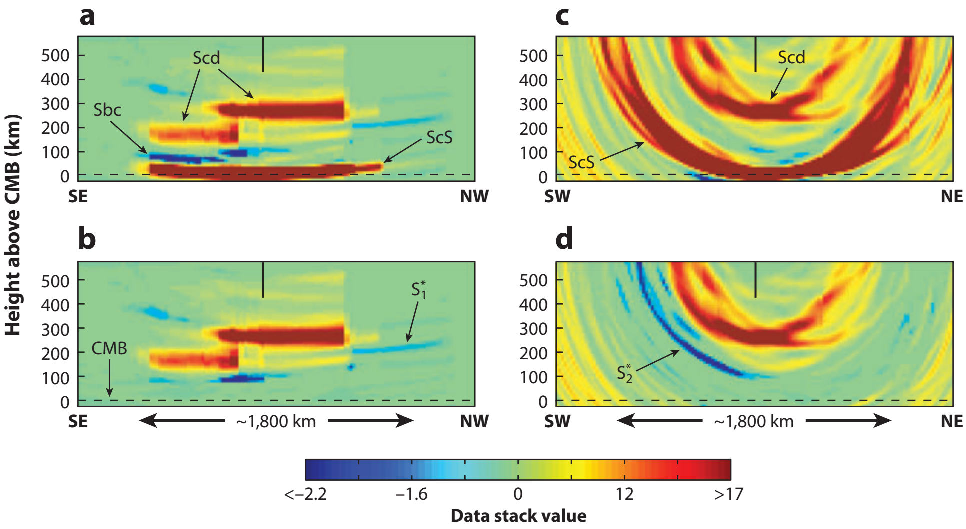

Figure 11

Cross sections through an SH wave point-source scattering migration model for the reflectivity of the lowermost mantle beneath the Cocos plate. The data ray paths trend from southeast to northwest and provide good resolution of structure in that direction (*a*, *b*), but strong isochronal artifacts in the perpendicular southwest-to-northeast cross sections give artifacts known as migration smiles (*c*, *d*). The black vertical lines at the top of each panel indicate the position of intersection. Panels *a* and *c* include the ScS arrivals, whereas these have been muted out in the migration shown in panels *b* and *d*. Red amplitudes indicate reflections from velocity increases other than at those the core-mantle boundary (CMB). Note the abrupt step in the reflector with a change in depth of almost 100 km. The negative reflections labeled S_1* and S_2* are interpreted as out-of-plane scattering from lateral gradients in structure rather than from horizontal velocity decreases, based on the asymmetry of the smile features in the southwest-to-northeast cross sections. From Hutko et al. (2006).

Thomas et al. (2004a) applied simple point-scatterer migration to small subsets of S waves sampling different areas beneath the Cocos plate using data like those shown in **Figure 4**. They found evidence for a variation as large as 150 km in the main D″ reflector depth over a few hundred kilometers laterally in a 700-km-long migration corridor, with a more intermittent deeper velocity reduction. Although Lay et al. (2004a) found that lateral variations in velocity structure led to strong trade-offs with apparent depth of the velocity discontinuity beneath the Cocos plate, Hutko et al. (2006) extended the SH migration in this region to a full migration of all source-receiver combinations (that are kinematically viable) and also preferred strong depth variations (**Figure 11**), as did Kito et al. (2007b) and Sun & Helmberger (2008). Strong trade-offs still exist between laterally varying volumetric velocity and depths of reflectors in migrated images that assume 1D structure. Thomas et al. (2004b) applied simplified migration to structure beneath Eurasia, mapping a sharp increase in S velocity 206–316 km above the CMB and a sharp reduction in S velocity 55–85 km above the CMB. The upper velocity increase corresponds to features detected in other modeling and stacking efforts, but the deeper decrease is subtle and corresponds to features similar to those that Thomas et al. (2004a) proposed under the Cocos plate. Hernlund et al. (2005) advanced the idea that the deeper decrease may involve reversal of the perovskite-to-postperovskite phase transition in a steep thermal gradient above the CMB. Because a velocity decrease will not produce any critical angle amplification associated with triplication, the inference of velocity decreases is subtle relative to velocity increases (Flores & Lay 2005, Sun & Helmberger

2008), especially if the velocity decrease is distributed over depth rather than acting as sharp reflectors. Caution must be taken to avoid incorrectly attributing postcritical phase distortions to negative reflectors for both double-array stacking and migrations; Hutko et al. (2006) pointed out that some features in the migration images of structure beneath the Cocos plate may be from localized scattering rather than velocity layering.

Improving the resolution of migration images when the source-receiver geometries are fixed usually involves development of stack weighting criteria. Kito et al. (2007a) proposed a slowness-backazimuth weighted migration (SBWM) that combines slowness, azimuth, and travel time weighting schemes with 3D point-scatterer migration, attempting to suppress artifacts from incomplete ray-path sampling (see **Figure 11**). Each grid point in the image volume has theoretical slowness and azimuth to each station in the receiver array, with corresponding range. A data time window is specified depending on the Fresnel zone of the dominant period (T/4), the receiver array aperture, and travel time differences among target phases. The data traces are shifted and summed, and the value is plotted on slowness and backazimuth coordinates relative to the receivers. Deviations between theoretical and observed slowness and backazimuth are calculated, and absolute values are projected into a Gaussian function; the result is used to weight from 0 to 1 the stack energy of the grid point. The weight functions are usually raised to some power and multiplied with the migrated signals, strongly suppressing signal energy that is inconsistent with point scattering from the target location. Such nonlinear weighting suppresses artifacts but also may lead to unrealistic assessment of structure detection capabilities. Relying on the image amplitudes to estimate structural properties is also difficult, and 3D modeling and migration of synthetic scattered phases need to be done before quantitative statements about the structure can be made.

Chambers & Woodhouse (2006a,b) applied weights based on slowness variations among the signals that contribute to each stack according to the generalized Radon transform, which governs the relationship between slant stacks of the data and the imaged structure. This is appealing because it retains the formal imaging resolution of seismic wavefields without any nonlinear weighting. They applied this approach to large sets of long-period waveforms that sample the deep mantle beneath northern Eurasia and North America. This procedure explicitly allows precritical and postcritical observations to be combined, as the changes in reflection coefficient strength and polarity can be accounted for as a function of wave slowness. The images are realistically smoothed (and blurry). Similar stacking with inverse Radon transform weighting and statistical corrections of the data have been performed by Wang et al. (2006), van der Hilst et al. (2007), and Wang et al. (2008) (see **Figure 12**). Large S-wave data sets with many signals were migrated for structure beneath North America in the first two studies, whereas more extensive coverage was provided by migrating global SKKS signals in Wang et al. (2008). Most of the data in these studies involve precritical reflection geometries, with only a small fraction having wide-angle triplication geometries. It is difficult to distinguish between artifacts and resolved features in huge data set migrations that include shallow earthquakes because the data may be complicated by strong crustal heterogeneity as well as by inclusion of many low-magnitude events with high noise levels. Confirmation (or believability) of any particular migration model feature is often established by the stability of features across different seismic studies and data sets for the same region. In many cases, results differ, and hence interpretations may be premature. The SKKS study attempted to detect underside precritical reflections from D″ layering that arrive after the SKKS core phase, which requires suppression of strong later arrivals such as SKKKS.

All deep mantle imaging has limited wave-path coverage, variability of earthquake source functions, and unexplained effects of heterogeneity outside the volume of interest, and simply processing larger numbers of signals might not overcome these obstacles. Seismogram quality control and preprocessing relative to clear reference phases are still advisable to ensure that signals

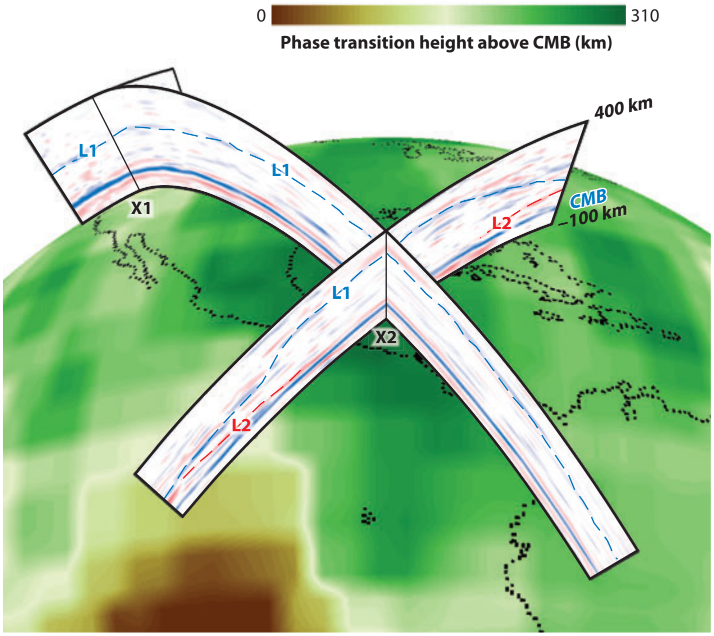

Figure 12

Cross sections intersecting at positions X1 and X2 through the large-scale S-wave migration model for the deep mantle under North America produced by van der Hilst et al. (2007) superimposed on a background that indicates inferred height of a phase transition with positive Clapeyron slope inferred from velocity heterogeneity by Sidorin et al. (1999). The core-mantle boundary (CMB) is apparent as the deepest blue stripe with adjacent red stripes (side-lobe artifacts). The features labeled L1 and L2 correspond to inferred continuous reflectors with velocity increases and decreases, respectively. There are many additional intermittent features that may be real or may be noise. The image has few migration smiles, in part because some regions have better azimuthal coverage than the corridor imaged in **Figure 11**, but also because the smiles have been arbitrarily truncated to emphasize energy near the turning point. From van der Hilst et al. (2007). Reprinted with permission from AAAS.

of interest are viably present below the noise level. This approach leads to smaller data sets, but the results are more reliable, as indicated by the greater agreement of results from different studies.

Kito & Korenaga (2010) attempted to enhance the resolution of small-scale structures imaged via point-scattering migration by cross-correlation of shifted seismograms rather than by weighting by azimuth and slowness. The basic strategy is to seek optimal scattering locations under the assumption of coherent wavelets isotropically radiating toward different receivers. This is dependent on the assumption of isotropic scattering, which is not implausible over small receiver separations, and holds promise relative to other, more time-consuming procedures such as SBWM. As with other methods, one must be cautious about ignoring forward-scattering radiation coefficients, postcritical phase shifts, and diffraction distortions. Further discussion of the technical aspects of these methods can be found in Rost & Thomas (2010).

Migration is particularly useful for detecting isolated weak scattering from mid-mantle heterogeneities that produce secondary arrivals that might otherwise go unrecognized due to their lack of standard 1D slowness move-out (Rost et al. 2008). Kito et al. (2008) applied the SBWM method to data from South American earthquakes recorded by Californian seismic networks to seek coherent arrivals in the late P coda arrivals. Apparent reflection locations extend from the transition zone down to the D″ region, concentrated beneath the Caribbean, although assessing the confidence level of the images is difficult. Kaneshima & Helffrich (2009) similarly sought scattered S-P arrivals in late P coda using a grid of potential scatterer locations extending from 800 to 2,200 km deep. They found 10 groups of scatterers below areas of present subduction, finding evidence for scattering from structures in the upper half of the lower mantle (but not clearly in the deep mantle). They attributed the scattering to lateral velocity gradients in slab material that has penetrated into the lower mantle. These methods are promising but require future quantification through the use of 3D synthetics and larger data sets.

Migration methods are intrinsic to most deterministic treatments of strongly scattered phases, such as precursors to PKIKP phases. These precursors can be generated near the CMB on either the source side or the receiver side of the path, within a kinematically restricted volume (Hedlin & Shearer 2000). Thomas et al. (1999) applied migration to precursor signals using $1° \times 1°$ grids in both scattering volumes, with amplitudes normalized on the peak precursor levels and with the use of Nth-root stacking. Cao & Romanowicz (2007) tried to locate PKP precursors using array analysis of earthquake doublets. Waveform modeling approaches for strongly scattered phases within kinematically constrained scattering volumes have been applied by Helmberger et al. (1998), Wen & Helmberger (1998), Cormier (1999), Wen (2000), Niu & Wen (2001), Miller & Niu (2008), and Thomas et al. (2009). Basic characteristics of the scattering fabrics have been modeled as a transition zone of the D″ heterogeneity spectrum (Cormier 2000).

INTERPRETATIONS OF DEEP MANTLE IMAGES

The seismologically imaged features in the deep mantle provide first-order information regarding structures and processes, but joint interpretation with mineral physics and geodynamics information is required to evaluate the thermochemical significance of the structures (e.g., Forte & Mitrovica 2001, Deschamps & Trampert 2003, Resovsky & Trampert 2003, Trampert et al. 2004). We briefly summarize primary interpretations, all of which are areas of ongoing research and continued improvement of imaging applications; collectively, they are coalescing into a new paradigm for deep mantle evolution (Garnero et al. 2007a, Garnero & McNamara 2008, Trønnes 2009).

Deep Mantle Discontinuities

The discovery in 2004 of a phase change in the primary lower-mantle mineral, magnesium silicate perovskite [$(Mg,Fe)SiO_3$] (Iitaka et al. 2004, Murakami et al. 2004), provides a plausible explanation for the P- and S-wave velocity discontinuities at the top of the D″ layer. The temperature and compositional dependency of this phase change and the predicted elasticity and transport properties of the high-pressure polymorph known as postperovskite provide the first predictive context for evaluating the seismological images (Lay et al. 2005, Wookey et al. 2005, Lay & Garnero 2007). For example, variations in depth of an abrupt shear velocity discontinuity can be related to relative temperature fluctuations (Helmberger et al. 2005, Sun & Helmberger 2008), paired discontinuities with opposite sign can be related to multiple intersections of the local geotherm with the phase boundary and with temperature gradients and heat flow (Hernlund et al. 2005, Lay et al. 2006, van der Hilst et al. 2007, Lay et al. 2008), and anisotropic properties can be predicted and compared with observations (e.g., Wookey et al. 2005, Kawai & Tsuchiya 2009). The observed seismic reflector in D″ appears to involve a velocity increase over less than 50 km in depth (Lay 2008), but the postperovskite phase transition may involve a two-phase regime as thick as 400–600 km (Catalli et al. 2009). This requires either that the bulk of the transition occurs over only a limited portion of the two-phase regime or that the seismic reflections are from a concentrated transition of anisotropic properties in postperovskite. The latter possibility has been considered by Ammann et al. (2010), who found that diffusion of Mg^{2+} and Si^{4+} in postperovskite is extremely anisotropic and that postperovskite may be much weaker than perovskite. Horizontal shear flows causing deformation in the weak material could concentrate a gradient in anisotropy, giving rise to seismic energy reflection.

Ultralow-Velocity Zones

The localized structure right at the CMB is highly variable, but widespread occurrence of ULVZs near the margins of LLSVPs in the deep mantle is becoming well-established (McNamara et al. 2010). The magnitude of the velocity reductions and relative effects on P- and S-wave velocity have been attributed to the presence of a melt phase. In addition, the possible role of partial melting in the deep mantle has many present-day thermal and dynamical implications (e.g., Lay et al. 2004b) as well as possible implications for dense melt segregation in a deep mantle magma ocean over all of Earth history (Labrosse et al. 2007). ULVZs may be a manifestation of very high iron content in a thin layer of subsolidus postperovskite (Mao et al. 2006), although it appears more likely that iron preferentially partitions into ferropericlase in the deep mantle. Wicks et al. (2010) found that sound velocities of very iron-rich $(Mg_{.16}Fe_{.84})O$ at ambient temperatures are remarkably low relative to silicates. They thus proposed that solid-state concentration of very iron-rich (Mg,Fe)O may be the cause of ULVZs. It remains an open issue as to whether iron enrichment could occur by chemical reactions and lateral infiltration of core materials at the CMB or whether there are iron-rich residues of core formation processes.

Large Low Shear wave Velocity Provinces

The extensive imaging of the LLSVPs under Africa and the Pacific, which has built on early low-resolution tomography detections of these regions, has established that their distinctive properties likely involve compositional heterogeneity. The sharp lateral gradients of these regions, their scale and morphology, and their elasticity (very low S-wave velocity, moderately low P-wave velocity, possible high density) are primary lines of evidence for this. Least certain is the inference of high density (Ishii & Tromp 1999, 2001), as this relies on complex interpretations of normal modes (Romanowicz 2001, Kuo & Romanowicz 2002). The LLSVP density is important with respect to whether these are large, buoyant, thermal "superplumes" or hot, dense piles of compositionally distinct material swept into their present configuration by surrounding downwellings and upwellings (Tan et al. 2002; McNamara & Zhong 2004, 2005). The spatial correlations between LLSVPs, ULVZs, surface hotspot volcanism, and global-mantle-tomography velocity variations imply a dynamical significance for the LLSVPs, but their roles are not fully resolved (McNamara et al. 2010). A strong correlation between the present-day configuration of LLSVPs and reconstructed emplacement locations for large igneous provinces dating back several hundred million years implies long-term stability of LLSVPs (Burke & Torsvik 2004; Torsvik et al. 2006, 2010; Wen 2006; Burke et al. 2008), although there is some indication of ongoing internal deformation within the LLSVPs (McNamara et al. 2003, Tan & Gurnis 2005, D. Sun et al. 2007). The longevity of large-scale structures of the deep mantle is highly relevant to history of the geodynamo, as it appears that lateral heat-flux boundary conditions may play a major role in long-term magnetic field behavior (Glatzmaier et al. 1999).

LIMITATIONS, UNCERTAINTIES, AND FUTURE DIRECTIONS

Lower-mantle imaging efforts are certainly improving as data sets accumulate and new seismic station deployments are undertaken. Although the imaging limitations intrinsic to such deep remote targets are unavoidable, the multiplicity of seismic phases that can be utilized provides a surprising degree of sampling and resolution of structures. However, sometimes expected phases are weak or have unexplained variability, so their use as references for detecting other arrivals can be compromised. If reference phases are not used, unmodeled 3D volumetric velocity heterogeneity can defocus secondary phases, projecting artifacts into the imaged volume. There is also increasing recognition of very strong lateral gradients in shallow structure, so failure to account for multipathing and receiver complexity can lead to erroneous interpretation of deep structure for all methods. This article has not addressed studies of deep mantle anisotropy, but it appears to exist in the D″ region, and that can complicate wavefield interactions and interpretations of stacked and migrated images.

The complexity of models for the deep mantle is steadily increasing, partly because of slowly expanding data coverage, but primarily because of increasingly optimistic inference of structural details based on very small features in data stacks and migration images. Continuing growth of the databases used in various studies partly justifies the greater detail, but the reliability of modeling very small features in 1D stacks or in 3D migration images that clearly have imaging artifacts is subject to debate. There is no question that the real structure has 3D variations, but we have limited knowledge of the precise heterogeneity spectrum in the deep mantle. Possibly the parameterizations of structures, the assumptions of dimensionality, and our ignorance of detailed near-source and near-receiver complexities are still blemishing our understanding of deep mantle structure.

With the gradual emergence of 3D numerical modeling capabilities, it should become possible to more thoroughly explore these effects and to process higher-frequency 3D wavefield simulations to better evaluate the actual performance of current stacking and migration approaches. Using small data sets of high-quality data to validate results based on large data sets of "noisy" data is needed. More intermediate-scale (50–100-km dimension) arrays of broadband sensors are also needed around the world to better sample fine-scale structures of the deep mantle.

CONCLUSIONS

Significant advances in our understanding of deep mantle structure have been made by exploiting large seismic data sets accumulated by permanent and transportable seismic stations and by processing these with new waveform modeling, stacking, and migration methods. Although resolution will always be limited by the great seismic wave-path lengths and relatively low frequencies involved in all data that sample the deep mantle, the intermediate-scale (10–200-km) roughness of various regions of deep mantle structure is being progressively imaged, and profound implications are emerging from the models. It appears that a major phase change, significant large-scale and long-enduring chemical heterogeneity, and likely occurrence of dense melts or iron-rich residues play major roles in deep mantle dynamics, heat transport, and chemical evolution. Refining global tomography is essential for improving the resolution of the smooth large-scale structures, which define the background structure for higher-resolution migration work, but many more applications of higher-resolution waveform analysis procedures are essential to resolving the rough structure that is directly sensitive to the detailed processes in the deep mantle.

DISCLOSURE STATEMENT

The authors are not aware of any affiliations, memberships, funding, or financial holdings that might be perceived as affecting the objectivity of this review.

ACKNOWLEDGMENTS

This work was supported by NSF Grants EAR-0635570 (T.L.) and EAR-0453944 (E.J.G.). We thank P. Lin for help in preparing **Figures 1**, **2**, and **7**.

LITERATURE CITED

Ammann MW, Brodholt JP, Wookey J, Dobson DP. 2010. First-principles constraints on diffusion in lower-mantle minerals and a weak D″ layer. *Nature* 465:462–65

Antolik M, Gu YJ, Ekström G. 2003. J362D28: a new joint model of compressional and shear velocity in the Earth's mantle. *Geophys. J. Int.* 153:443–66

Avants M, Lay T, Garnero EJ. 2006a. A new probe of ULVZ S-wave velocity structure: array stacking of ScS waveforms. *Geophys. Res. Lett.* 33:L07314

Avants M, Lay T, Russell SA, Garnero EJ. 2006b. Shear velocity variation within the D″ region beneath the Central Pacific. *J. Geophys. Res.* 111:B05305

Bilek SL, Lay T. 1998. Lower mantle heterogeneity beneath Eurasia imaged by parametric migration of shear waves. *Phys. Earth Planet. Inter.* 108:201–18

Braña L, Helffrich G. 2004. A scattering region near the core-mantle boundary under the North Atlantic. *Geophys. J. Int.* 158:625–636

Bréger L, Romanowicz B, Ng C. 2001. The Pacific plume as seen by S, ScS, and SKS. *Geophys. Res. Lett.* 28:1859–62

Buffett BA, Garnero EJ, Jeanloz R. 2000. Sediments at the top of Earth's core. *Science* 290:1338–42

Bullen KE. 1949. Compressibility-pressure hypothesis and the Earth's interior. *MNRAS Geophys. Suppl.* 5:355–68

Burke K. Steinberger B, Torsvik TH, Smethurst MA. 2008. Plume generation zones at the margins of large low shear velocity provinces on the core-mantle boundary. *Earth Planet. Sci. Lett.* 265:49–60

Burke K, Torsvik TH. 2004. Derivation of large igneous provinces of the past 200 million years from long-term heterogeneities in the deep mantle. *Earth Planet. Sci. Lett.* 227:531–38

Cao A, Romanowicz B. 2007. Locating scatterers in the mantle using array analysis of PKP precursors from an earthquake doublet. *Earth Planet. Sci. Lett.* 255:22–31

Castle JC, Creager KC, Winchester JP, van der Hilst RD. 2000. Shear wave speeds at the base of the mantle. *J. Geophys. Res.* 105:21543–57

Castle JC, van der Hilst RD. 2000. The core-mantle boundary under the Gulf of Alaska: no ULVZ for shear waves. *Earth Planet. Sci. Lett.* 176:311–21

Castle JC, van der Hilst RD. 2003. Using ScP precursors to search for mantle structures beneath 1800 km depth. *Geophys. Res. Lett.* 30(8):1422

Catalli K, Shim S-H, Prakapenka V. 2009. Thickness and Clapeyron slope of the postperovskite boundary. *Nature* 462:782–785

Chaloner J, Thomas C, Rietbrock A. 2009. P- and S-wave reflectors in D″ beneath South-East Asia. *Geophys. J. Int.* 179:1080–92

Chambers K, Woodhouse JH. 2006a. Investigating the lowermost mantle using migrations of long-period *S–ScS* data. *Geophys. J. Int.* 166:667–78

Chambers K, Woodhouse JH. 2006b. Transient D″ discontinuity revealed by seismic migration. *Geophys. Res. Lett.* 33:L17312

Cormier VF. 1999. Anisotropy of heterogeneity scale lengths in the lower mantle from PKIKP precursors. *Geophys. J. Int.* 136:373–84

Cormier VF. 2000. D″ as a transition in the heterogeneity spectrum of the lowermost mantle. *J. Geophys. Res.* 105:16193–205

Deschamps F, Trampert J. 2003. Mantle tomography and its relation to temperature and composition. *Phys. Earth Planet. Inter.* 140:272–91

Dziewonski AM, Anderson DL. 1981. Preliminary reference Earth model. *Phys. Earth Planet. Inter.* 25:297–356

Fisher JL, Wysession ME, Fischer KM. 2003. Small-scale lateral variations in D″ attenuation and velocity structure. *Geophys. Res. Lett.* 30(8):1435

Flores C, Lay T. 2005. The trouble with seeing double. *Geophys. Res. Lett.* 32:L24305

Ford SR, Garnero EJ, McNamara AK. 2006. A strong lateral shear velocity gradient and anisotropy heterogeneity in the lowermost mantle beneath the southern Pacific. *J. Geophys. Res.* 111:B03306

Forte AM, Mitrovica JX. 2001. Deep-mantle high-viscosity flow and thermochemical structure inferred from seismic and geodynamic data. *Nature* 410:1049–56

Freybourger M, Chevrot S, Krüger F, Achauer U. 2001. A waveform migration for the investigation of P wave structure at the top of D″ beneath northern Siberia. *J. Geophys. Res.* 106:4129–40

Gaherty JB, Lay T. 1992. Investigation of laterally heterogeneous shear velocity structure in D″ beneath Eurasia. *J. Geophys. Res.* 97:417–35

Garnero EJ. 2000. Heterogeneity of the lowermost mantle. *Annu. Rev. Earth Planet. Sci.* 28:509–37

Garnero EJ, Jeanloz R. 2000. Fuzzy patches on the Earth's core-mantle boundary. *Geophys. Res. Lett.* 27:2777–80

Garnero EJ, Lay T. 2003. D″ shear velocity heterogeneity, anisotropy and discontinuity structure beneath the Caribbean and Central America. *Phys. Earth Planet. Inter.* 140:219–42

Garnero EJ, Lay T, McNamara AK. 2007a. Implications of lower-mantle structural heterogeneity for existence and nature of whole-mantle plumes. *Geol. Soc. Am. Spec. Pap.* 430:79–91

Garnero EJ, McNamara AK. 2008. Structure and dynamics of Earth's lower mantle. *Science* 320:626–28

Garnero EJ, Thorne MS, McNamara A, Rost S. 2007b. Fine-scale ultra-low velocity zone layering at the core-mantle boundary and superplumes. In *Superplumes: Beyond Plate Tectonics*, ed. DA Yuen, S Maruyama, SI Karato, BF Windley, pp. 139–58. New York: Springer

Garnero EJ, Vidale JE. 1999. ScP; a probe of ultralow velocity zones at the base of the mantle. *Geophys. Res. Lett.* 26:377–80

Glatzmaier GA, Coe RS, Hongre L, Roberts PH. 1999. The role of the Earth's mantle in controlling the frequency of geomagnetic reversals. *Nature* 401:885–90

Grand SP. 2002. Mantle shear-wave tomography and the fate of subducted slabs. *Philos. Trans. R. Soc. A* 360:2475–91

Gu YJ, Dziewonski AM, Su W, Ekström G. 2001. Models of the mantle shear velocity and discontinuities in the pattern of lateral heterogeneities. *J. Geophys. Res.* 106:11169–99

Havens E, Revenaugh J. 2001. A broadband seismic study of the lowermost mantle beneath Mexico: constraints on ultralow velocity zone elasticity and density. *J. Geophys. Res.* 106:30809–20

He Y, Wen L. 2009. Structural features and shear-velocity structure of the "Pacific Anomaly." *J. Geophys. Res.* 114:B02309

He Y, Wen L, Zheng T. 2006. Geographic boundary and shear wave velocity structure of the "Pacific anomaly" near the core-mantle boundary beneath western Pacific. *Earth Planet. Sci. Lett.* 244:302–14

Hedlin MAH, Shearer PM. 2000. An analysis of large-scale variations in small-scale mantle heterogeneity using Global Seismographic Network recordings of precursors to *PKP*. *J. Geophys. Res.* 105:13655–73

Helmberger DV, Lay T, Ni S, Gurnis M. 2005. Deep mantle structure and the postperovskite phase transition. *Proc. Natl. Acad. Sci. USA* 102(48):17257–63

Helmberger DV, Ni S. 2005. Approximate 3D body-wave synthetics for tomographic models. *Bull. Seismol. Soc. Am.* 9:212–24

Helmberger DV, Ni S, Wen L, Ritsema J. 2000. Seismic evidence for ultralow velocity zones beneath Africa and eastern Atlantic. *J. Geophys. Res.* 105:23865–78

Helmberger DV, Wen L, Ding X. 1998. Seismic evidence that the source of the Iceland hotspot lies at the core-mantle boundary. *Nature* 396:251–55

Hernlund JW, Thomas C, Tackley PJ. 2005. A doubling of the postperovskite phase boundary and structure of the Earth's lowermost mantle. *Nature* 434:882–86

Hung SH, Garnero EJ, Chiao LY, Kuo BY, Lay T. 2005. Finite-frequency tomography of D″ shear velocity heterogeneity beneath the Caribbean. *J. Geophys. Res.* 110:B07305

Hutko A, Lay T, Garnero EJ, Revenaugh JS. 2006. Seismic detection of folded, subducted lithosphere at the core-mantle boundary. *Nature* 441:333–36

Hutko AR, Lay T, Revenaugh J. 2009. Localized double-array stacking analysis of PcP: *D″* and ULVZ structure beneath the Cocos plate, Mexico, central Pacific, and north Pacific. *Phys. Earth Planet. Inter.* 173:60–74

Hutko A, Lay T, Revenaugh J, Garnero EJ. 2008. Anticorrelated seismic velocity anomalies from postperovskite in the lowermost mantle. *Science* 320:1070–74

Idehara K, Yamada A, Zhao D. 2007. Seismological constraints on the ultralow velocity zones in the lowermost mantle from core-reflected waves. *Phys. Earth Planet. Inter.* 165:25–46

Iitaka T, Hirose K, Kawamura K, Murakami M. 2004. The elasticity of the $MgSiO_3$ postperovskite phase in the Earth's lowermost mantle. *Nature* 430:442–44

Ishii M, Tromp J. 1999. Normal-mode and free-air gravity constraints on lateral variations in velocity and density of Earth's mantle. *Science* 285:1231–36

Ishii M, Tromp J. 2001. Even-degree lateral variations in the Earth's mantle constrained by free oscillations and the free-air gravity anomaly. *Geophys. J. Int.* 145:77–96

Kaneshima S, Helffrich G. 1998. Detection of lower mantle scatterers northeast of the Mariana subduction zone using short-period array data. *J. Geophys. Res.* 103:4825–38

Kaneshima S, Helffrich G. 2009. Lower mantle scattering profiles and fabric below Pacific subduction zones. *Earth Planet. Sci. Lett.* 282:234–39

Kawai K, Geller RJ. 2010. Waveform inversion for localized seismic structure and an application to D′′ structure beneath the Pacific. *J. Geophys. Res.* 115:B01305

Kawai K, Geller RJ, Fuji N. 2007a. D′′ beneath the Arctic from inversion of shear waveforms. *Geophys. Res. Lett.* 34:L21305

Kawai K, Sekine S, Fuji N, Geller RJ. 2009. Waveform inversion for D′′ structure beneath northern Asia using Hi-net tiltmeter data. *Geophys. Res. Lett.* 36:L20314

Kawai K, Takeuchi N, Geller RJ, Fuji N. 2007b. Possible evidence for a double crossing phase transition in D′′ beneath Central America from inversion of seismic waveforms. *Geophys. Res. Lett.* 34:L09314

Kawai K, Tsuchiya T. 2009. Temperature profile in the lowermost mantle from seismological and mineral physics joint modeling. *Proc. Natl. Acad. Sci. USA* 106:22119–23

Kellogg LH, Hager BH, van der Hilst RD. 1999. Compositional stratification in the deep mantle. *Science* 283:1881–84

Kito T, Korenaga J. 2010. Cross-correlation weighted migration: towards high resolution mapping of mantle heterogeneities. *Geophys. J. Int.* 181:1109–27

Kito T, Krüger F. 2001. Heterogeneities in D′′ beneath the southwestern Pacific inferred from scattered and reflected P-waves. *Geophys. Res. Lett.* 28:2545–48

Kito T, Krüger F, Negishi H. 2004. Seismic heterogeneous structure in the lowermost mantle beneath the southwestern Pacific. *J. Geophys. Res.* 109:B09304

Kito T, Rietbrock A, Thomas C. 2007a. Slowness-backazimuth weighted migration: a new array approach to a high-resolution image. *Geophys. J. Int.* 169:1201–9

Kito T, Rost S, Thomas C, Garnero EJ. 2007b. New insights into the *P*- and *S*-wave velocity structure of the D′′ discontinuity beneath the Cocos plate. *Geophys. J. Int.* 169:631–45

Kito T, Thomas C, Rietbrock A, Garnero EJ, Nippress SEJ, Heath AE. 2008. Seismic evidence for a sharp lithospheric base persisting to the lowermost mantle beneath the Caribbean. *Geophys. J. Int.* 174:1019–28

Konishi K, Kawai K, Geller RJ, Fuji N. 2009. MORB in the lowermost mantle beneath the western Pacific: evidence from waveform inversion. *Earth Planet. Sci. Lett.* 278:219–25

Krüger F, Scherbaum F, Weber M, Schlittenhardt J. 1996. Analysis of asymmetric multipathing with a generalization of the double-beam method. *Bull. Seismol. Soc. Am.* 86:737–49

Krüger F, Weber M, Scherbaum F, Schlittenhardt J. 1993. Double beam analysis of anomalies in the core-mantle boundary region. *Geophys. Res. Lett.* 20:1475–78

Krüger F, Weber M, Scherbaum F, Schlittenhardt J. 1995. Normal and inhomogeneous lowermost mantle and core-mantle boundary under the Arctic and Northern Canada. *Geophys. J. Int.* 122:637–58

Kuo BY, Garnero EJ, Lay T. 2000. Tomographic inversion of *S-SKS* times for shear velocity heterogeneity in D′′: degree 12 and hybrid models. *J. Geophys. Res.* 105:28139–57

Kuo C, Romanowicz B. 2002. On the resolution of density anomalies in the Earth's mantle using spectral fitting of normal-mode data. *Geophys. J. Int.* 150:162–79

Kustowski B, Ekström G, Dziewonski AM. 2008. Anisotropic shear-wave velocity structure of the Earth's mantle: a global model. *J. Geophys. Res.* 113:B06306

Labrosse S, Hernlund JW, Coltice N. 2007. A crystallizing dense magma ocean at the base of the Earth's mantle. *Nature* 450:866–69

Lay T. 2008. Sharpness of the D′′ discontinuity beneath the Cocos Plate: implications for the perovskite to postperovskite phase transition. *Geophys. Res. Lett.* 35:L03304

Lay T, Garnero EJ. 2004. Core-mantle boundary structures and processes. In *The State of the Planet: Frontiers and Challenges in Geophysics*, ed. RSJ Sparks, CJ Hawkesworth, *Geophys. Monogr.* 150:25–41. Washington, DC: AGU

Lay T, Garnero EJ. 2007. Reconciling the postperovskite phase with seismological observations of lowermost mantle structure. In *Post-Perovskite: The Last Mantle Phase Transition*, ed. K Hirose, J Brodholt, T Lay, D Yuen, *Geophys. Monogr.* 174:129–53. Washington, DC: AGU

Lay T, Garnero EJ, Russell S. 2004a. Lateral variation of the D′′ discontinuity beneath the Cocos Plate. *Geophys. Res. Lett.* 31:L15612

Lay T, Garnero EJ, Williams Q. 2004b. Partial melting in a thermo-chemical boundary layer at the base of the mantle. *Phys. Earth Planet. Inter.* 146:441–67

Lay T, Heinz D, Ishii M, Shim S-H, Tsuchiya T, et al. 2005. Multidisciplinary impact of the lower mantle perovskite phase transition. *Eos Trans. AGU* 86(1):1, 5

Lay T, Helmberger DV. 1983a. A lower mantle *S*-wave triplication and the velocity structure of D′′. *Geophys. J. R. Astron. Soc.* 75:799–837

Lay T, Helmberger DV. 1983b. The shear wave velocity gradient at the base of the mantle. *J. Geophys. Res.* 88:8160–70

Lay T, Hernlund J, Buffett BA. 2008. Core-mantle boundary heat flow. *Nat. Geosci.* 1:25–32

Lay T, Hernlund J, Garnero EJ, Thorne MS. 2006. A postperovskite lens and *D*′′ heat flux beneath the central Pacific. *Science* 314:1272–76

Lay T, Young CJ. 1996. Imaging scattering structures in the lower mantle by migration of long-period S waves. *J. Geophys. Res.* 101:20023–40

Li C, van der Hilst RD, Engdahl ER, Burdick W. 2008. A new global model for *P* wave speed variations in Earth's mantle. *Geochem. Geophys. Geosyst.* 9:Q05018

Luo SN, Ni SD, Helmberger DV. 2001. Evidence for a sharp lateral variation of velocity at the core-mantle boundary from multipathed PKPab. *Earth Planet. Sci. Lett.* 189:155–64

Mao WL, Mao HK, Sturhahn W, Zhao J, Prakapenka VB, et al. 2006. Iron-rich postperovskite and the origin of ultralow-velocity zones. *Science* 312:564–65

McNamara AK, Garnero EJ, Rost S. 2010. Tracking deep mantle reservoirs with ultra-low velocity zones. *Earth Planet. Sci. Lett.* 299:1–9

McNamara AK, van Keken PE, Karato SI. 2003. Development of finite strain in the convecting lower mantle and its implications for seismic anisotropy. *J. Geophys. Res.* 108(B5):2230

McNamara AK, Zhong S. 2004. Thermochemical structures within a spherical mantle: superplumes or piles? *J. Geophys. Res.* 109:B07402

McNamara AK, Zhong S. 2005. Thermochemical structures beneath Africa and the Pacific Ocean. *Nature* 437:1136–39

Megnin C, Romanowicz B. 2000. The three-dimensional shear velocity structure of the mantle from the inversion of body, surface and higher-mode waveforms. *Geophys. J. Int.* 143:709–28

Miller MS, Niu F. 2008. Bulldozing the core-mantle boundary: localized seismic scatterers beneath the Caribbean Sea. *Phys. Earth Planet. Int.* 170:89–94

Murakami M, Hirose K, Kawamura K, Sata N, Ohishi Y. 2004. Postperovskite phase transition in $MgSiO_3$. *Science* 304:855–58

Ni S, Ding X, Helmberger DV. 2000. Constructing synthetics from deep earth tomographic models. *Geophys. J. Int.* 14:71–82

Ni S, Helmberger DV. 2003a. Seismological constraints on the South African superplume; could be the oldest distinct structure on earth. *Earth Planet. Sci. Lett.* 206:119–31

Ni S, Helmberger DV. 2003b. Ridge-like lower mantle structure beneath South Africa. *J. Geophys. Res.* 108(B2):2094

Ni S, Helmberger DV, Tromp J. 2005. Three-dimensional structure of the Africa superplume from waveform modeling. *Geophys. J. Int.* 161:283–94

Ni S, Tan E, Gurnis M, Helmberger DV. 2002. Sharp sides to the African superplume. *Science* 296:1850–52
Niu F, Wen L. 2001. Strong seismic scatterers near the core-mantle boundary west of Mexico. *Geophys. Res. Lett.* 24:3557–60
Ohta K, Hirose K, Lay T, Sata N, Ohishi Y. 2008. Phase transitions in pyrolite and MORB at lowermost mantle conditions: implications for a MORB-rich pile above the core-mantle boundary. *Earth Planet. Sci. Lett.* 267:107–17
Panning M, Romanowicz B. 2006. A three-dimensional radially anisotropic model of shear velocity in the whole mantle. *Geophys. J. Int.* 167:361–79
Persch SE, Vidale JE, Earle PS. 2001. Absence of short-period ULVZ precursors to PcP and ScP from two regions of the CMB. *Geophys. Res. Lett.* 28:387–90
Reasoner C, Revenaugh J. 1999. Short-period P-wave constraints on D″ reflectivity. *J. Geophys. Res.* 10:955–61
Reasoner C, Revenaugh J. 2000. ScP constraints on ultralow velocity zone density and gradient thickness beneath the Pacific. *J. Geophys. Res.* 105:28173–82
Resovsky J, Trampert J. 2003. Using probabilistic seismic tomography to test mantle velocity-density relationships. *Earth Planet. Sci. Lett.* 215:121–34
Revenaugh JS, Meyer R. 1997. Seismic evidence of partial melt within a possibly ubiquitous low-velocity layer at the base of the mantle. *Science* 277:670–73
Ritsema J, Garnero E, Lay T. 1997. A strongly negative shear velocity gradient in the lowermost mantle beneath the Pacific. *J. Geophys. Res.* 102:20395–411
Ritsema J, Ni S, Helmberger DV, Crotwell HP. 1998. Evidence for strong shear velocity reductions and velocity gradients in the lower mantle beneath Africa. *Geophys. Res. Lett.* 25:4245–48
Ritsema J, van Heijst HJ. 2000. Seismic imaging of structural heterogeneity in Earth's mantle: evidence for large-scale mantle flow. *Sci. Prog.* 83:243–59
Romanowicz B. 2001. Can we resolve 3D density heterogeneity in the lower mantle? *Geophys. Res. Lett.* 28:1107–10
Rondenay S, Cormier VF, Van Ark EM. 2010. *SKS* and *SPdKS* sensitivity to two-dimensional ultralow-velocity zones. *J. Geophys. Res.* 115:B04311
Rondenay S, Fischer KM. 2003. Constraints on localized core-mantle boundary structure from multichannel, broadband *SKS* coda analysis. *J. Geophys. Res.* 108:2537
Rost S, Garnero EJ, Stefan W. 2010a. Thin and intermittent ultralow-velocity zones. *J. Geophys. Res.* 115:B06312
Rost S, Garnero EJ, Thorne MS, Hutko AR. 2010b. On the absence of an ultralow-velocity zone in the North Pacific. *J. Geophys. Res.* B04312
Rost S, Garnero EJ, Williams Q. 2006. Fine-scale ultralow-velocity zone structure from high-frequency seismic array data. *J. Geophys. Res.* 111:B09310
Rost S, Garnero EJ, Williams Q. 2008. Seismic array detection of subducted oceanic crust in the lower mantle. *J. Geophys. Res.* 113:B06303
Rost S, Garnero EJ, Williams Q, Manga M. 2005. Seismic constraints on a possible plume root at the core-mantle boundary. *Nature* 435:666–69
Rost S, Revenaugh J. 2001. Seismic detection of rigid zones at the top of the core. *Science* 294:1911–14
Rost S, Revenaugh J. 2003. Small-scale ultralow-velocity zone structure imaged by *ScP*. *J. Geophys. Res.* 108:2056
Rost S, Thomas C. 2002. Array seismology: methods and applications. *Rev. Geophys.* 40:1–27
Rost S, Thomas C. 2010. High resolution CMB imaging from migration of short-period core reflected phases. *Phys. Earth Planet. Inter.* 183:143–50
Russell SA, Reasoner C, Lay T, Revenaugh J. 2001. Coexisting shear- and compressional-wave seismic velocity discontinuities beneath the central Pacific. *Geophys. Res. Lett.* 28:2281–84
Saltzer RL, van der Hilst RD, Kárason H. 2001. Comparing *P* and *S* wave heterogeneity in the mantle. *Geophys. Res. Lett.* 28:1335–38
Scherbaum F, Krüger F, Weber M. 1997. Double beam imaging: mapping lower mantle heterogeneities using combinations of source and receiver arrays. *J. Geophys. Res.* 102:507–22
Schimmel M, Paulssen H. 1997. Noise reduction and detection of weak, coherent signals through phase-weighted stack. *Geophys. J. Int.* 130:497–505

Sidorin I, Gurnis M, Helmberger DV. 1999. Evidence for a ubiquitous seismic discontinuity at the base of the mantle. *Science* 286:1326–31

Simmons NA, Grand SP. 2002. Partial melting in the deepest mantle. *Geophys. Res. Lett.* 29:1552

Stutzmann E, Vinnik L, Ferreira A, Singh S. 2000. Constraint on the S-wave velocity at the base of the mantle. *Geophys. Res. Lett.* 27:1571–74

Sun D, Helmberger D. 2008. Lower mantle tomography and phase change mapping. *J. Geophys. Res.* 113:B10305

Sun D, Helmberger D, Gurnis M. 2010. A narrow, mid-mantle plume below southern Africa. *Geophys. Res. Lett.* 37:L09302

Sun D, Helmberger D, Ni S, Bower D. 2009. Direct measures of lateral velocity variation in the deep Earth. *J. Geophys. Res.* 114:B05303

Sun D, Song TRA, Helmberger D. 2006. Complexity of D′′ in the presence of slab-debris and phase changes. *Geophys. Res. Lett.* 33:L12S07

Sun D, Tan E, Helmberger DV, Gurnis M. 2007. Seismological support for the metastable superplume model, sharp features, and phase changes within the lower mantle. *Proc. Natl. Acad. Sci. USA* 104:9151–55

Sun X, Song X, Zheng S, Helmberger DV. 2007. Evidence for a chemical-thermal structure at base of mantle from sharp lateral P-wave variations beneath Central America. *Proc. Natl. Acad. Sci. USA* 104:26–30

Takeuchi N. 2007. Whole mantle SH velocity model constrained by waveform inversion based on three-dimensional Born kernels. *Geophys. J. Int.* 169:1153–63

Takeuchi N, Morita Y, Xuyen ND, Zung NQ. 2008. Extent of the low-velocity region in the lowermost mantle beneath the western Pacific detected by the Vietnamese Broadband Seismograph Array. *Geophys. Res. Lett.* 35:L05307

Tan E, Gurnis M. 2005. Metastable superplumes and mantle compressibility. *Geophys. Res. Lett.* 32:L20307

Tan E, Gurnis M, Han L. 2002. Slabs in the lower mantle and their modulation of plume formation. *Geochem. Geophys. Geosyst.* 3:11067

Tanaka S. 2002. Very low shear wave velocity at the base of the mantle under the South Pacific superswell. *Earth Planet. Sci. Lett.* 203:879–93

Thomas C, Garnero EJ, Lay T. 2004a. High-resolution imaging of lowermost mantle structure under the Cocos Plate. *J. Geophys. Res.* 109:B08307

Thomas C, Heesom T, Kendall JM. 2002. Investigating the heterogeneity of the D′′ region beneath the northern Pacific using a seismic array. *J. Geophys. Res.* 107(B11):2274

Thomas C, Kendall JM, Helffrich G. 2009. Probing two low-velocity regions with *PKP* b-caustic amplitudes and scattering. *Geophys. J. Int.* 178:503–12

Thomas C, Kendall JM, Lowman J. 2004b. Lower-mantle seismic discontinuities and the thermal morphology of subducted slabs. *Earth Planet. Sci. Lett.* 225:105–13

Thomas C, Weber M, Wicks CW, Scherbaum F. 1999. Small scatterers in the lower mantle observed at German broadband arrays. *J. Geophys. Res.* 104:15073–88

Thorne MS, Garnero EJ. 2004. Inferences on ultralow-velocity zone structure from a global analysis of *SPdKS* waves. *J. Geophys. Res.* 109:B08301

Thorne MS, Garnero EJ, Grand SP. 2004. Geographic correlation between hot spots and deep mantle lateral shear-wave velocity gradients. *Phys. Earth Planet. Inter.* 146:47–63

Thorne MS, Lay T, Garnero EJ, Jahnke G, Igel H. 2007. Seismic imaging of the laterally varying D′′ region beneath the Cocos Plate. *Geophys. J. Int.* 170:635–48

To A, Romanowicz B, Capdeville Y, Takeuchi N. 2005. 3D effects of sharp boundaries at the borders of the African and Pacific Superplumes: observation and modeling. *Earth Planet Sci. Lett.* 233:137–53

Torsvik TH, Burke K, Steinberger B, Webb SJ, Ashwal LD. 2010. Diamonds sampled by plumes from the core-mantle boundary. *Nature* 466:352–55

Torsvik TH, Smethurst MA, Burke K, Steinberger B. 2006. Large igneous provinces generated from the margins of the large low-velocity provinces in the deep mantle. *Geophys. J. Int.* 167:1447–60

Trampert J, Deschamps F, Resovsky J, Yuen D. 2004. Probabilistic tomography maps chemical heterogeneities throughout the lower mantle. *Science* 306:853–56

Trønnes RG. 2009. Structure, mineralogy and dynamics of the lowermost mantle. *Mineral. Petrol.* 99:243–61 van der Hilst RD, de Hoop MV, Wang P, Shim SH, Ma P, Tenoria L. 2007. Seismostratigraphy and thermal structure of Earth's core-mantle boundary region. *Science* 315:1813–17

van der Hilst RD, Kárason H. 1999. Compositional heterogeneity in the bottom 1000 kilometers of Earth's mantle: toward a hybrid convection model. *Science* 283:1885–88

Wallace M, Thomas C. 2005. Investigating D′′ structure beneath the North Atlantic. *Phys. Earth Planet. Inter.* 151:115–27

Wang P, de Hoop MV, van der Hilst RD. 2008. Imaging of the lowermost mantle (D′′) and the core-mantle boundary with SKKS coda waves. *Geophys. J. Int.* 175:103–15

Wang P, de Hoop MV, van der Hilst RD, Ma P, Tenorio L. 2006. Imaging of structure at and near the core-mantle boundary using a generalized radon transform: 1. Construction of image gathers. *J. Geophys. Res.* 111:B12304

Wang Y, Wen L. 2004. Mapping the geometry and geographic distribution of a very low velocity province at the base of the Earth's mantle. *J. Geophys. Res.* 109:B10305

Wang Y, Wen L. 2007. Geometry and P and S velocity structures of the "African Anomaly." *J. Geophys. Res.* 112:B05313

Weber M, Davis JP, Thomas C, Krüger F, Scherbaum F, et al. 1996. The structure of the lowermost mantle as determined from using seismic arrays. In *Seismic Modeling of the Earth's Structure*, ed. E Boschi, G Ekström, A Morelli, pp. 399–442. Rome: Inst. Naz. Geophys.

Wen L. 2000. Intense seismic scattering near the Earth's core-mantle boundary beneath the Comoros hotspot. *Geophys. Res. Lett.* 27:3627–30

Wen L. 2001. Seismic evidence for a rapidly varying compositional anomaly at the base of the Earth's mantle beneath the Indian ocean. *Earth Planet. Sci. Lett.* 194:83–95

Wen L. 2002. An *SH* hybrid method and shear velocity structures in the lowermost mantle beneath the central Pacific and South Atlantic Oceans. *J. Geophys. Res.* 107(B3):2055

Wen L. 2006. A compositional anomaly at the Earth's core-mantle boundary as an anchor to the relatively slowly moving surface hotspots and as source to the DUPAL anomaly. *Earth Planet. Sci. Lett.* 246:138–48

Wen L, Helmberger DV. 1998. Ultra-low velocity zones near the core-mantle boundary from broadband PKP precursors. *Science* 279:1701–3

Wen L, Silver P, James D, Kuehnel R. 2001. Seismic evidence for a thermo-chemical boundary layer at the base of the Earth's mantle. *Earth Planet. Sci. Lett.* 189:141–53

Wicks JK, Jackson JM, Sturhahn W. 2010. Very low sound velocities in iron-rich (Mg,Fe)O: implications for the core-mantle boundary region. *Geophys. Res. Lett.* 37:L15304

Wookey J, Stackhouse S, Kendall JM, Brodholt J, Price GD. 2005. Efficacy of the postperovskite phase as an explanation for lowermost-mantle seismic properties. *Nature* 438:1004–7

Wright C, Kuo BY. 2007. The P-wavespeed structure in the lowermost 700 km of the mantle below the central part of the Indian Ocean. *Phys. Earth Planet. Inter.* 161:243–66

Wysession ME, Fischer KM, Al-Eqabi GI, Shore PJ, Gurari I. 2001. Using MOMA broadband array *ScS-S* data to image smaller-scale structures at the base of the mantle. *Geophys. Res. Lett.* 28:867–70

Xu Y, Koper KD. 2009. Detection of a ULVZ at the base of the mantle beneath the northwest Pacific. *Geophys. Res. Lett.* 36:L17301

Yamada A, Nakanishi I. 1996. Detection of P-wave reflection in D′′ beneath the south-western Pacific using double-array stacking. *Geophys. Res. Lett.* 23:1553–56

Yamada A, Nakanishi I. 1998. Short-wavelength lateral variation of a D′′ P-wave reflector beneath the south-western Pacific. *Geophys. Res. Lett.* 25:4545–48

Young CJ, Lay T. 1990. Multiple phase analysis of the shear velocity structure in the D′′ region beneath Alaska. *J. Geophys. Res.* 95:17385–402

Zhao D. 2004. Global tomographic images of mantle plumes and subducting slabs: insight into deep Earth dynamics. *Phys. Earth Planet. Inter.* 146:3–34

Annual Review of Earth and Planetary Sciences

Volume 39, 2011

Contents

Indexes

Errata

An online log of corrections to *Annual Review of Earth and Planetary Sciences* articles may be found at http://earth.annualreviews.org